Bolt Beranek and Newman Inc.

Report No. 3532

The SRB Heat Shield: Aeroelastic Stability During Reentry

C. S. Ventres, E. H. Dowell

September 1977

Prepared for:
National Aeronautics and Space Administration

BBN Report No. 3532

THE SRB HEAT SHIELD: AEROELASTIC STABILITY DURING REENTRY

by

C.S. Ventres
E.H. Dowell

Prepared under Contract No. NAS8-32171

by

Bolt Beranek and Newman Inc.
Cambridge, Massachusetts 02138

for

National Aeronautics and Space Administration
George C. Marshall Space Flight Center
Marshall Space Flight Center, Alabama 35812

PREFACE

This is Volume I of a two volume final report for NASA Contract No. NAS8-32171 entitled, "SRB Reentry Acoustic Environment and Flexible Heat Shield Similarity Verification." In this volume, we report on those aspects of the program bearing upon the aeroelastic stability of the SRB heat shield during reentry. Our assessment of the reentry acoustic environment, along with a derivation and discussion of the relevant scaling parameters, is presented in Volume II.

The authors would like to acknowledge many helpful discussions with W.W. Clever and E.H. Walker of NASA MSFC. Their cooperation and assistance throughout the program is appreciated.

TABLE OF CONTENTS

TABLE OF CONTENTS *(Cont.)*

LIST OF FIGURES AND TABLES

LIST OF FIGURES AND TABLES *(Cont.)*

I. INTRODUCTION

The heat shield on the Solid Rocket Booster (SRB) is a fabric curtain that covers the annular opening between the lower edge of the aft skirt and the gimbeled rocket nozzle. Its primary purpose is to protect components within the cavity between the skirt and the nozzle from heat radiated by the exhaust plume during ascent, but it also reduces fluctuating pressure levels within the same cavity during reentry. A schematic drawing of the aft end of the SRB including the heat shield is shown in Fig. 1.

The SRB tumbles after being separated from the Orbiter, and then settles into a tail-down attitude as it reenters the atmosphere. Maximum dynamic pressure is reached when the reentry Mach number is about 2.75. During this critical phase of reentry, the angle between the longitudinal axis of the booster and the relative wind varies between 110° and 180°, with the aft end falling foremost. The heat shield is thus directly exposed to a supersonic flow at high dynamic pressure.

Wind tunnel tests of a 3% scale model of the aft portion of the SRB equipped with partially scaled heat shields were conducted for the purpose of measuring fluctuating pressure levels in the aft skirt region.* During these tests, the heat shields were observed to oscillate violently, the oscillations in some instances causing the heat shields to fail. High speed films taken during the tests reveal a regular pattern of waves in the fabric starting

*The mass/unit area of the model heat shields bore the proper relationship to full scale. Other similarity parameters bearing upon forced or self-excited aeroelastic response were not scaled. Mass-ratio scaling is appropriate for modelling the "mass law" response of an essentially limp membrane to enforced fluctuating pressure loads.

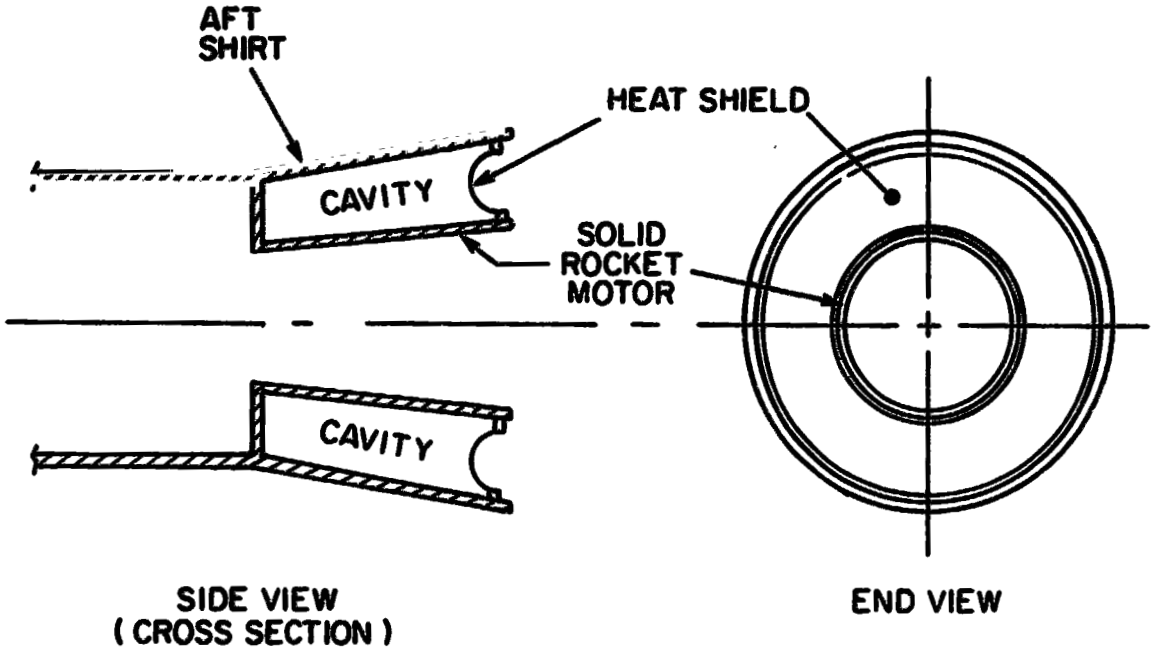

FIG. 1. SCHEMATIC OF AFT END OF SRB.

near the flow stagnation point and progressing around both sides of the annulus. The amplitude of the waves was too great, and their pattern too regular, for them to be attributed to the fluctuating pressure levels measured during the tests.

The purpose of the investigation reported here is to determine the cause of the oscillations observed in the model heat shields, and to determine whether or not similar oscillations will occur in the full scale SRB heat shield during reentry. Suggestions for modifying the heat shield so as to avoid the oscillations are provided, and recommendations are made for a program of vibration and wind tunnel tests of reduced-scale aeroelastic models of the heat shield. The recommended program provides an enhanced level of confidence in establishing a heat shield design that will survive reentry and provide protection for components contained within the aft skirt cavity.

2. QUASI-STEADY AERODYNAMIC ENVIRONMENT DURING REENTRY

Data on the expected reentry trajectories of the SRB have been provided by NASA Marshall Space Flight Center (Gallaboff, 1976). Of most importance to the present investigation are the predicted maximum values of dynamic pressure and the predicted attitude or angle of attack of the SRB during reentry. The maximum dynamic pressure (to be exceeded during only 5% of reentries) is shown in Fig. 2 as a function of reentry Mach number M_∞. The greatest dynamic pressure is encountered when the reentry Mach number is about 2.75.

During the portion of reentry at which maximum dynamic pressure is encountered, each SRB is expected to be executing a coning motion with an angle of attack greater than 90°. That is, the boosters fall nozzle-end first (see sketch in Fig. 3). The angle of attack is not constant, but varies randomly about an equilibrium value. The angle of attack is expected to fall outside the range shown in Fig. 3 during only 5% of all SRB reentries.

Even though the angle of attack is basically a random variable during reentry, the rate of variation of angle of attack is very small compared to the frequencies of the acoustic and aeroelastic disturbances being addressed in this report, so the flow around the aft end of the SRB can be assumed to be quasi-steady; that is, identical to the steady flow that would exist at the same instantaneous angle of attack. We can therefore infer the basic features of the flow over the aft skirt region of the SRB from the Schlieren photographs and time-averaged pressure data recorded during wind tunnel testing of a 3% scale model in the 1.02m × 1.02m (40 in × 40 in) Supersonic Wind Tunnel (A) at the Arnold Engineering Development Center (AEDC).

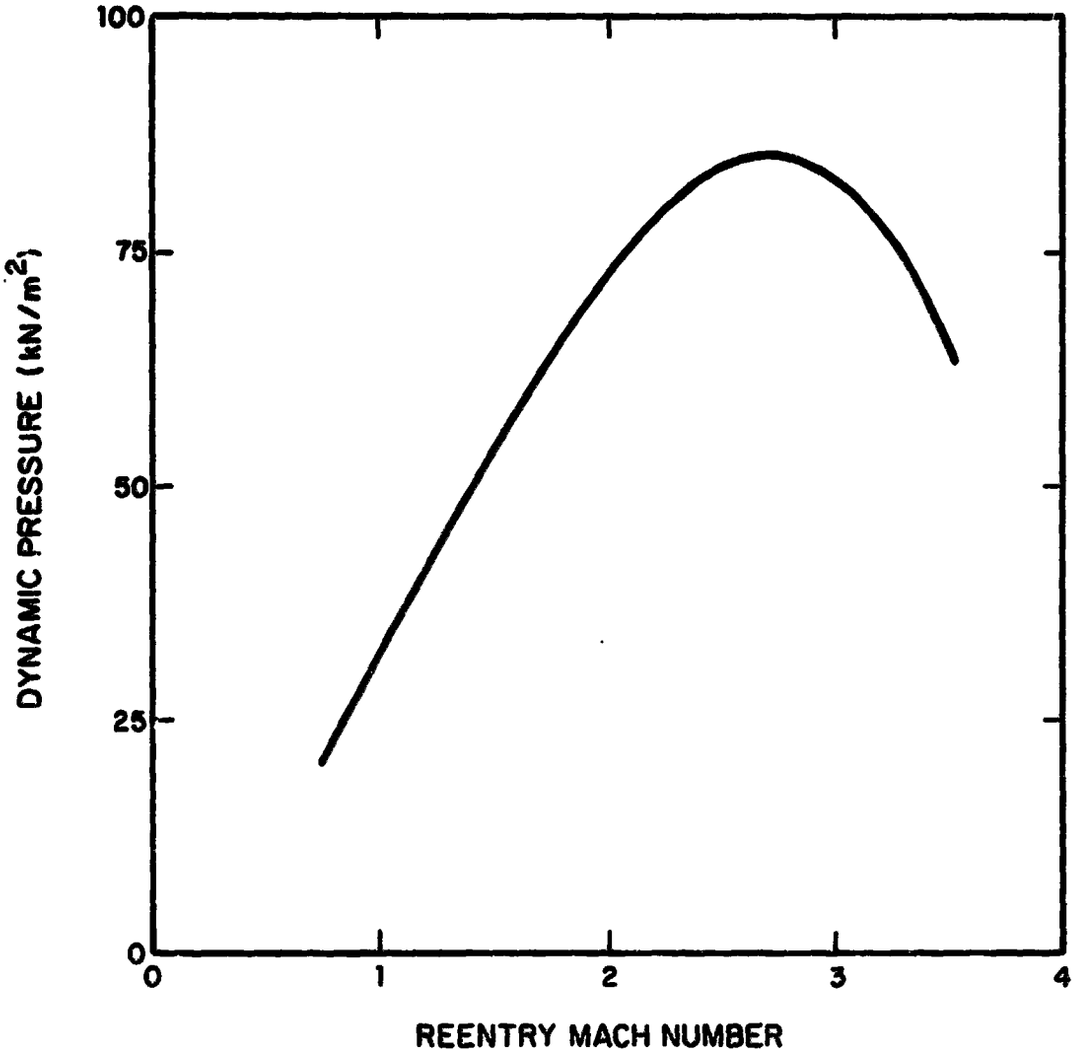

FIG. 2. DYNAMIC PRESSURE VS MACH NUMBER DURING REENTRY

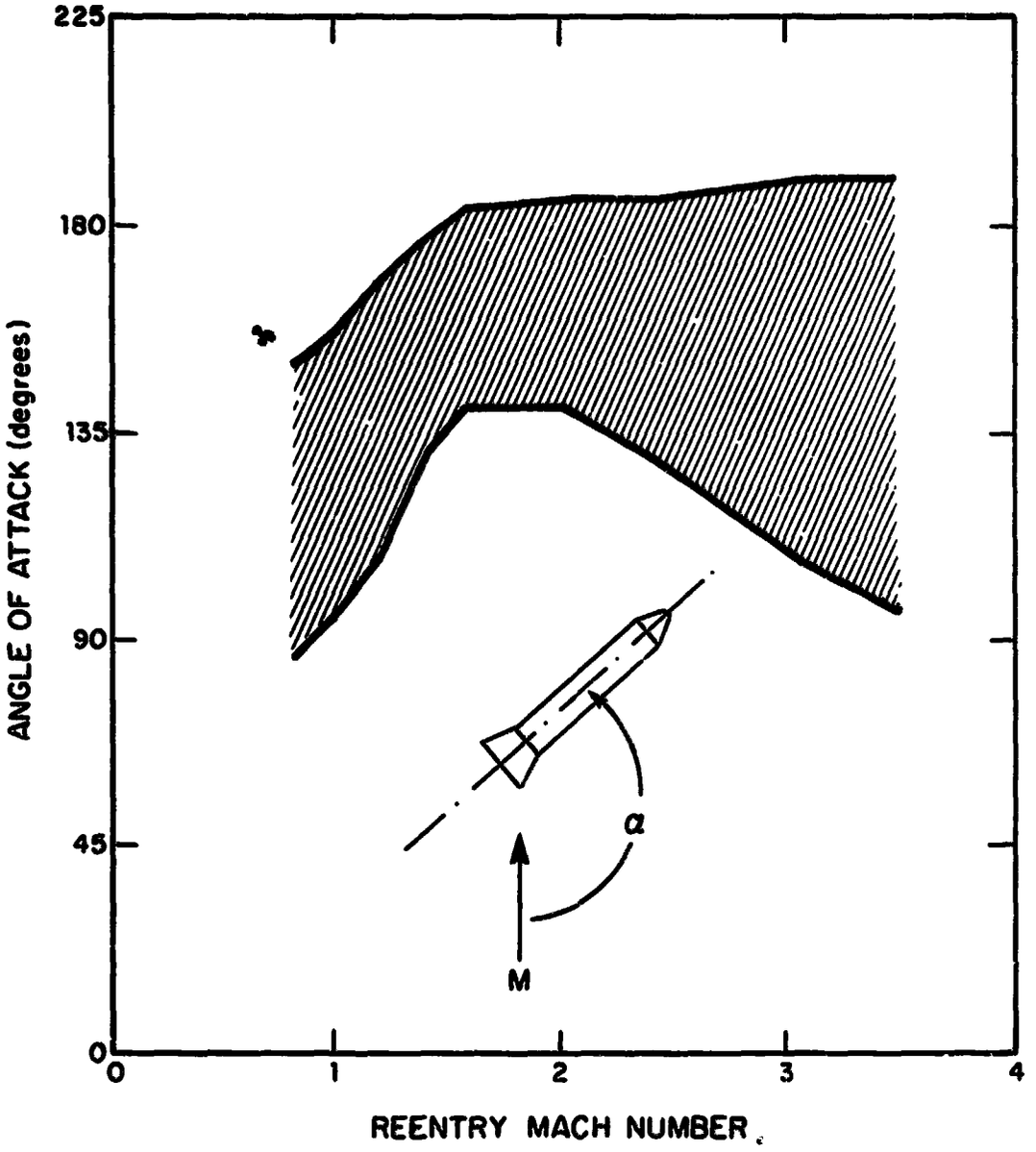

FIG. 3. ANGLE OF ATTACK RANGE DURING REENTRY

These tests were conducted at Mach numbers of 2.75 and 3.5. The angle of attack range was 110° to 139°. The test program was designed to determine *maximum* acoustic loads, so the test procedure was to record only rms pressure levels at selected points in the aft skirt region over the *entire* angle of attack range. Schlieren photographs were taken only at those angles of attack which produced the highest rms pressure fluctuations, so the shock structure is not known at all angles of attack. However, the available Schlieren of photographs show the situation depicted in Fig. 4.

At the angles of attack at which the greatest aeroelastic response and acoustic loads occurred an oblique shock wave was attached to the lip of the aft skirt at the stagnation point. In all cases checked, the angle formed by this shock wave with the direction of flow agreed (within ±1°) with that predicted by inviscid compressible flow theory for the two-dimensional flow over a wedge having the flow deflection angle θ shown in the figure. This was interpreted as evidence that, at least in the plane of lateral symmetry, the flow was essentially a 2-D wedge flow. To confirm this, time-averaged (DC) pressures recorded at several locations on the face of the aft skirt were plotted vs. angle of attack. Typical results are shown in Figs. 5 and 6 (M_∞ = 2.75 and 3.5, respectively). In each figure, the solid line is the pressure that would exist on the face of a wedge that turned the flow through the angle $\theta = \alpha - 90°$. The lines are extended only to the angle at which the shock would detach from the leading edge in a 2-D flow. At higher angles of attack, the shock will stand off from the skirt, and the flow will be subsonic over some or all of the face of the skirt.

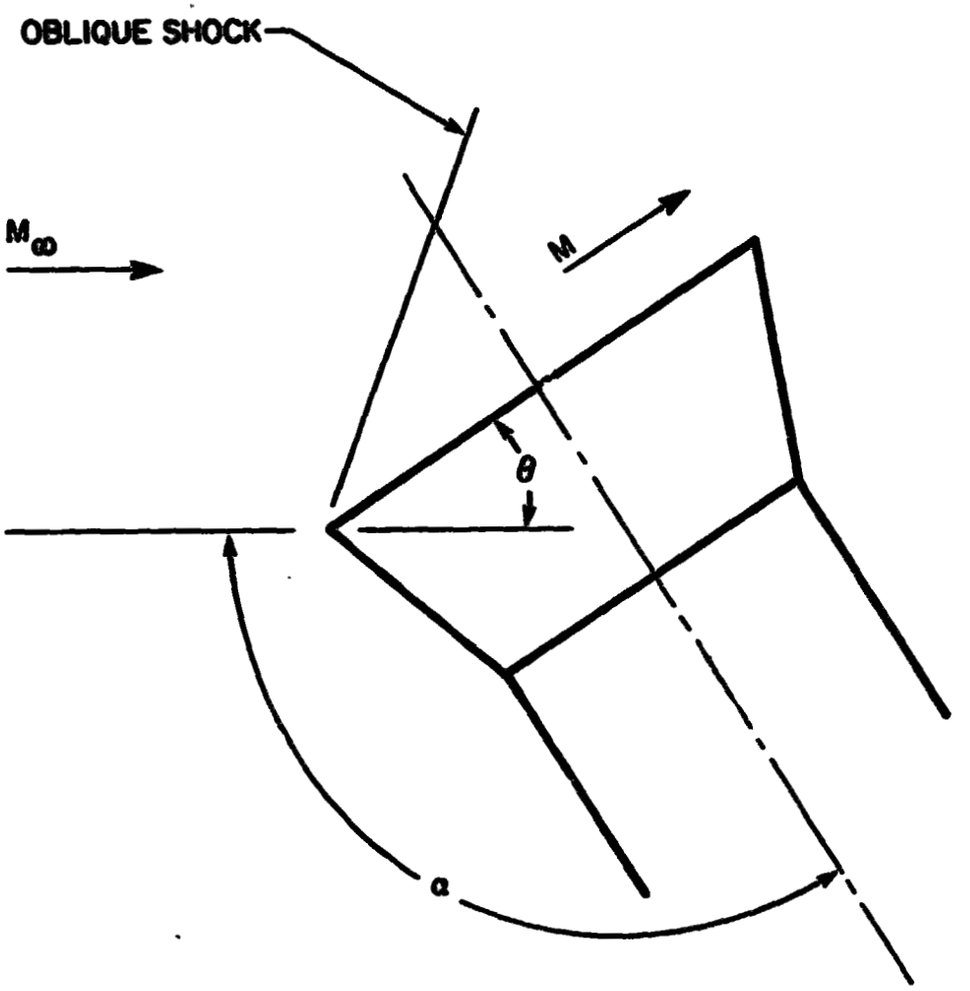

FIG. 4. LOCAL FLOW GEOMETRY

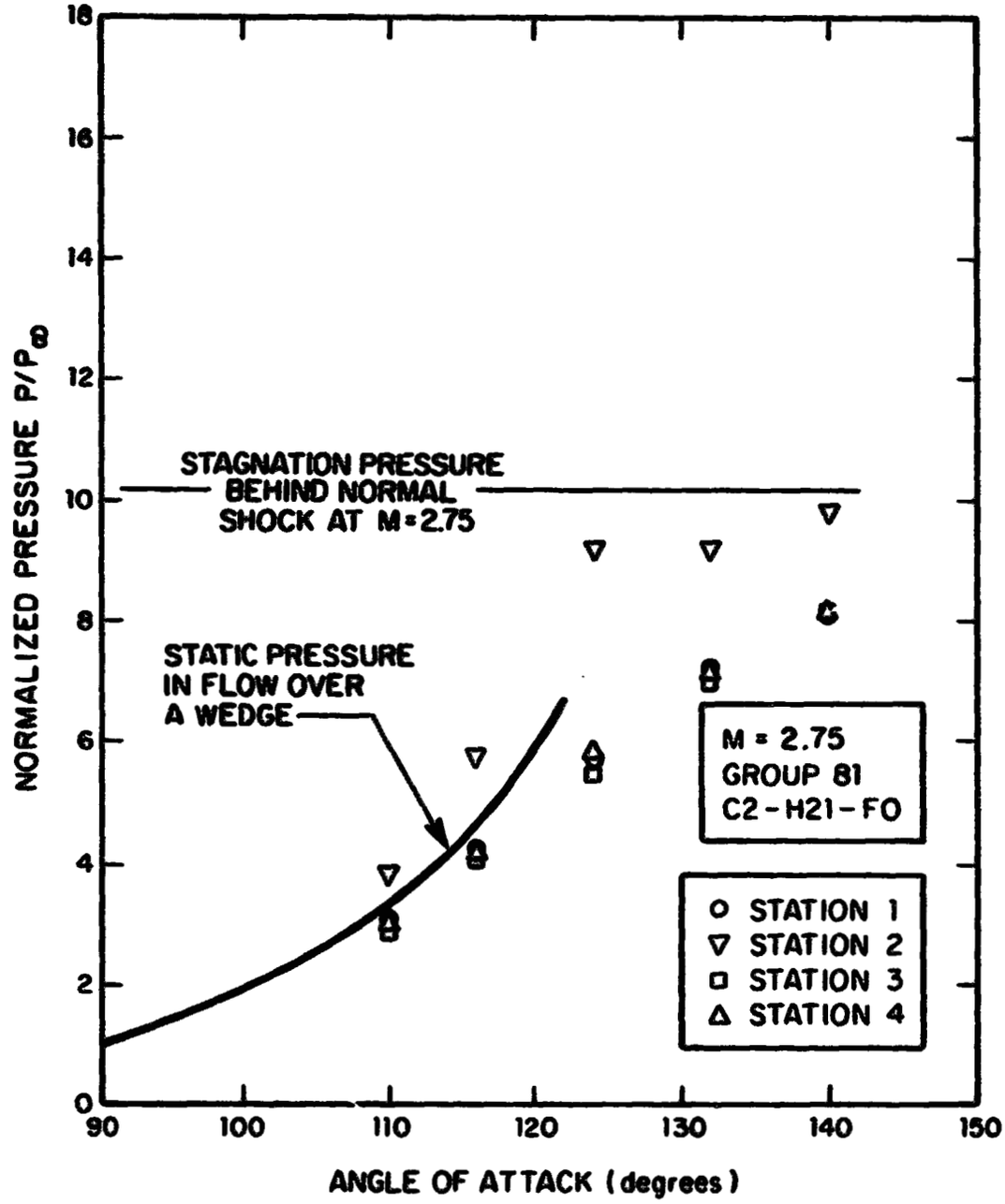

FIG. 5. STEADY PRESSURE OVER AFT SKIRT REGION, M_∞ = 2.75

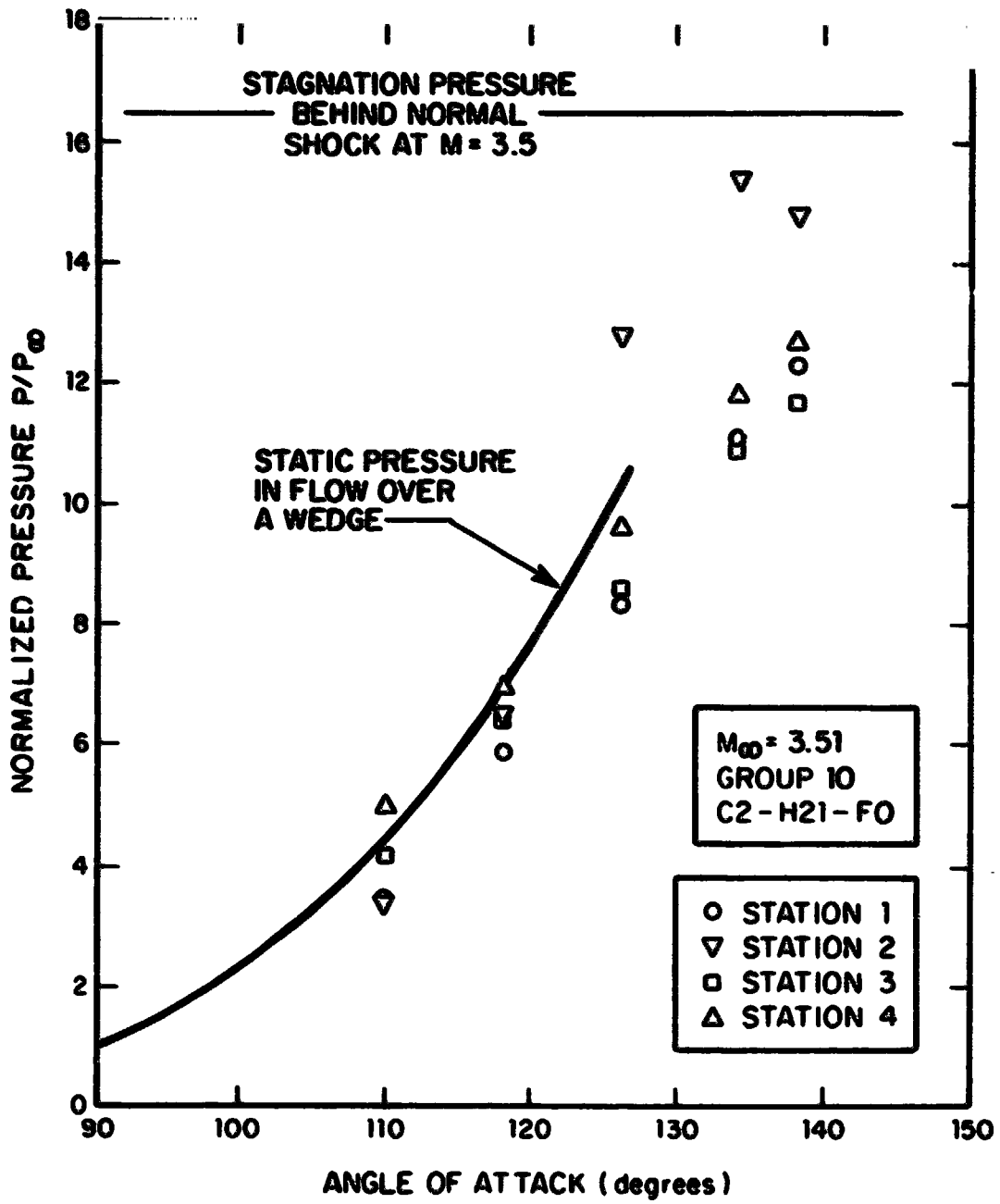

FIG. 6. STEADY PRESSURE OVER AFT SKIRT REGION, M_∞ = 3.51

The locations of transducers 1 through 4 are shown in Fig. 7* (locations P1 through P4). Transducer #2 is located immediately upstream of a small lip extending around the periphery of the truncated rocket nozzle. At high angles of attack, this transducer would be expected to read stagnation pressure, as indeed it is apparently doing in both figures for $\alpha > 120°$. The other transducers, however, show reasonable agreement with the wedge flow pressure curve for all angles less than the shock detachment angle.

In the following sections, we will assume that mean flow conditions over the face of the heat shield and the skirt proper can be related to free stream conditions by computing the flow over a wedge at the appropriate upstream Mach number and turning angle. The requisite theory and formulae are given in Liepman and Roshko (1957) and in NACA Report 1135 (1953), and will not be repeated here. For the present, we show in Figs. 8 and 9 the local Mach number and local dynamic pressure (normalized by the free stream value) as functions of angle of attack and free stream Mach number. These figures apply equally to any geometrically scaled wind tunnel model, and to the SRB itself. For the model, of course, M_∞ and q_∞ denote wind tunnel test section conditions, whereas at full scale they are the reentry Mach number and dynamic pressure.

To understand the aeroelastic oscillations of the heat shield, it is important to understand the following two points, implicit in Figs. 8 and 9:

---

*Figure taken from Porter (1976).

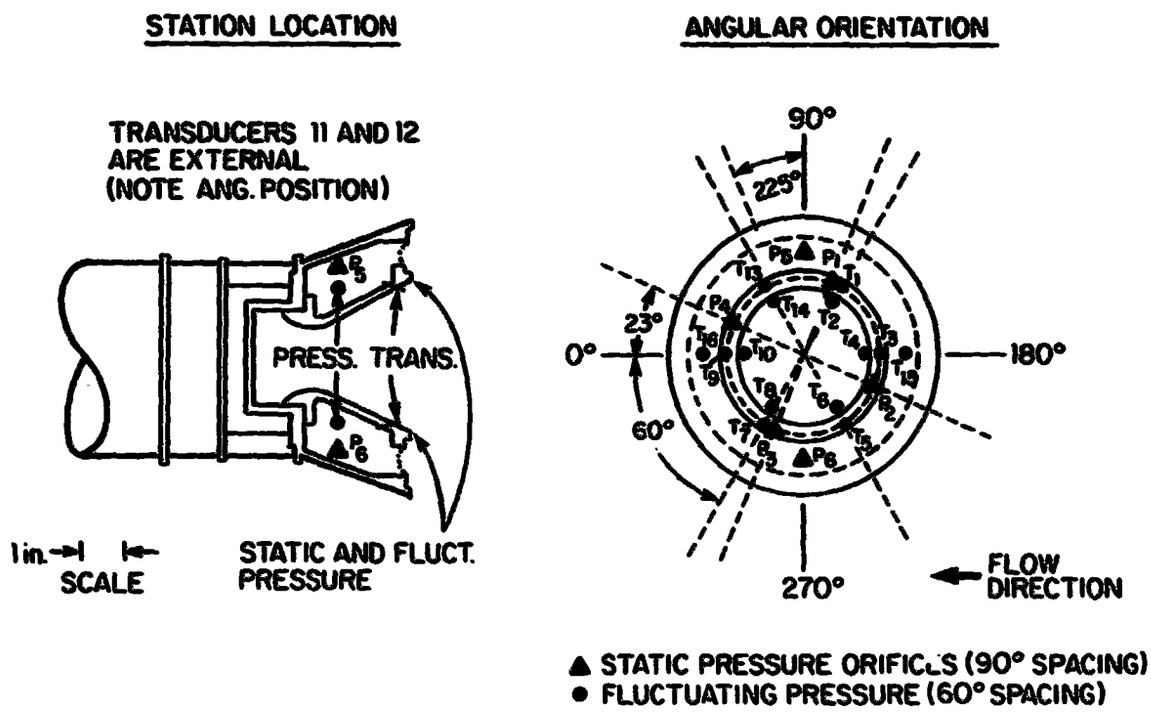

FIG. 7. SCHEMATIC OF 3% MODEL SHOWING LOCATION OF STATIC AND DYNAMIC TRANSDUCERS

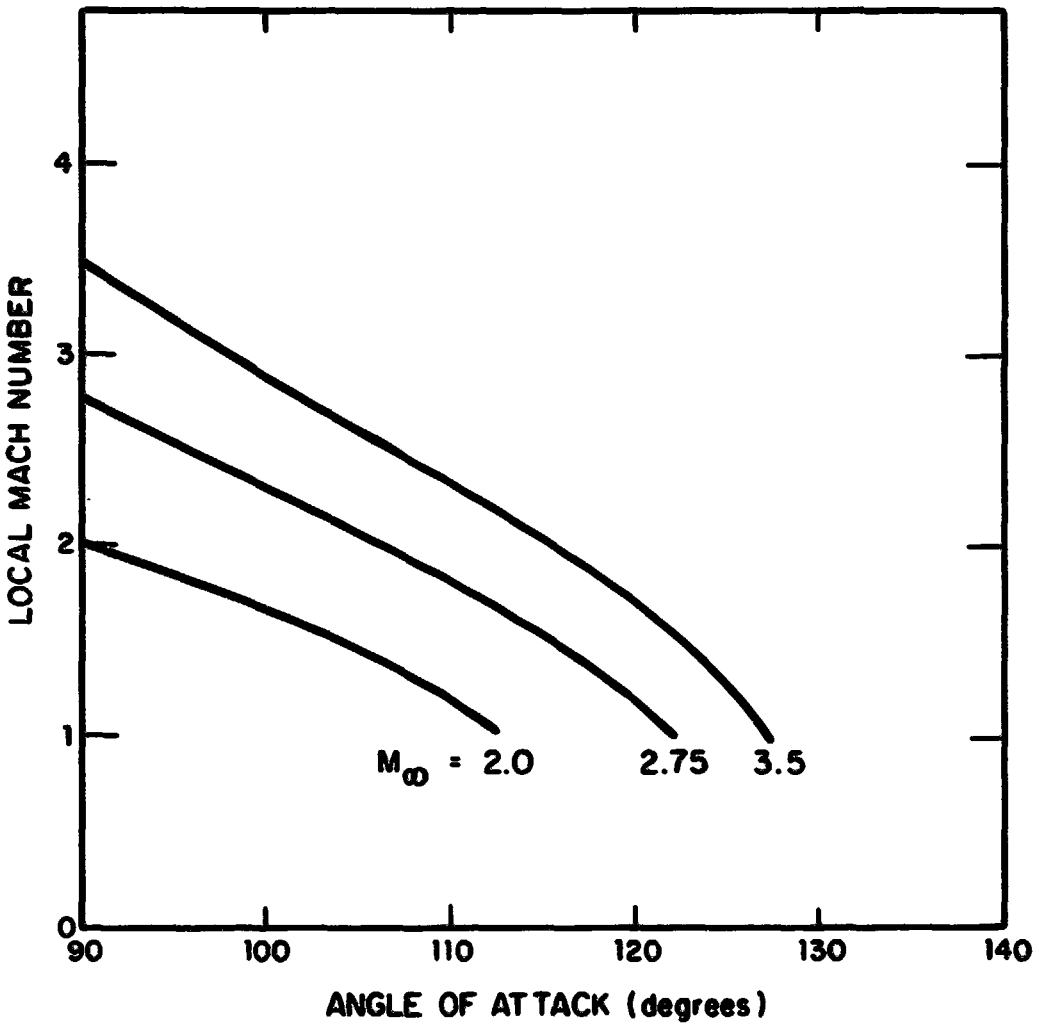

FIG. 8. LOCAL MACH NUMBER OVER FACE OF HEAT SHIELD

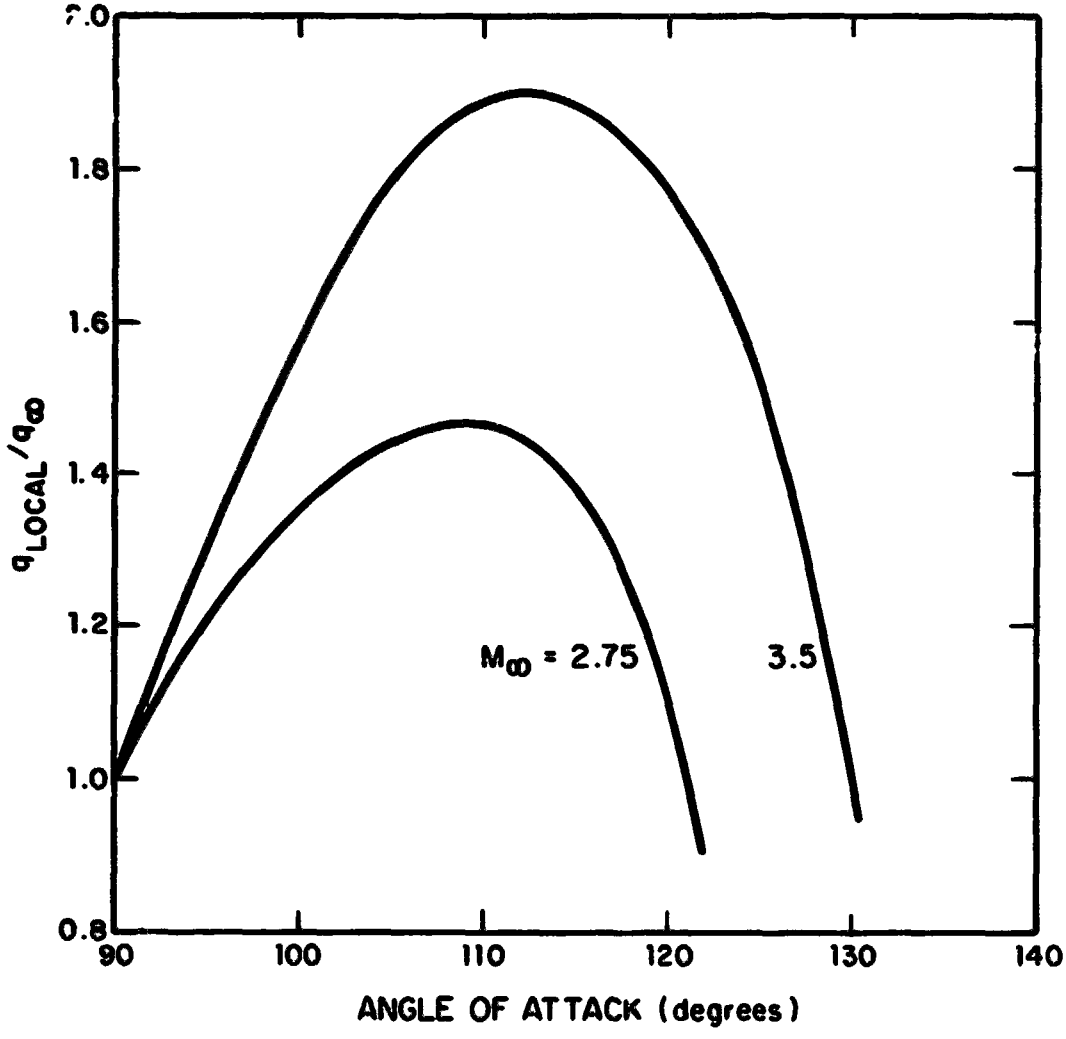

FIG. 9 NORMALIZED LOCAL DYNAMIC PRESSURE OVER FACE OF HEAT SHIELD

(1) The local Mach number over the heat shield is always less than or equal to the free stream Mach number. As the angle of attack increases from 90°, the local Mach number drops from the free stream value to 1.0. At still higher angles of attack, the flow over some portion or all of the heat shield is subsonic.

(2) The local dynamic pressure may exceed the free stream value, in spite of the viscous losses that occur in the oblique shock. By comparing the two figures, it can be seen that even where $M_\infty = 3.5$, the greatest *local* dynamic pressures occur at a *local* Mach number between 1.0 and 2.0.

Anticipating later results, the aeroelastic response of the heat shield is expected to be most severe w .n the local Mach number exceeds 1. As shown in Fig. 10, the local Mach number is expected to exceed 1 only when the reentry Mach number is greater than 2.6. *This potentially troublesome regime could be eliminated entirely if the expected angle of attack range could be narrowed for descent Mach numbers greater than 2.6.* To eliminate locally sypersonic velocities over the heat shield during the entire reentry, it would be necessary to insure that the angle of attack exceeds 132° at $M_\infty = 2.75$ and 137° at $M_\infty = 3.5$. Since the local Mach number is very sensitive to changes in angle of attack near $M_{local} = 1$, the angles quoted above incorporate a safety factor of 10°. That is, the theory predicts that $M_{local} = 1$ when $\alpha = 122°$ for $M_\infty = 2.75$, and when $\alpha = 127°$ for $M_\infty = 3.5$.

Elimination of locally supersonic flow over the heat shield will not preclude the possibility of unacceptable heat shield oscillations, but it will reduce their severity. The additicnal structural stiffness required to eliminate the oscillations will be correspondingly reduced.

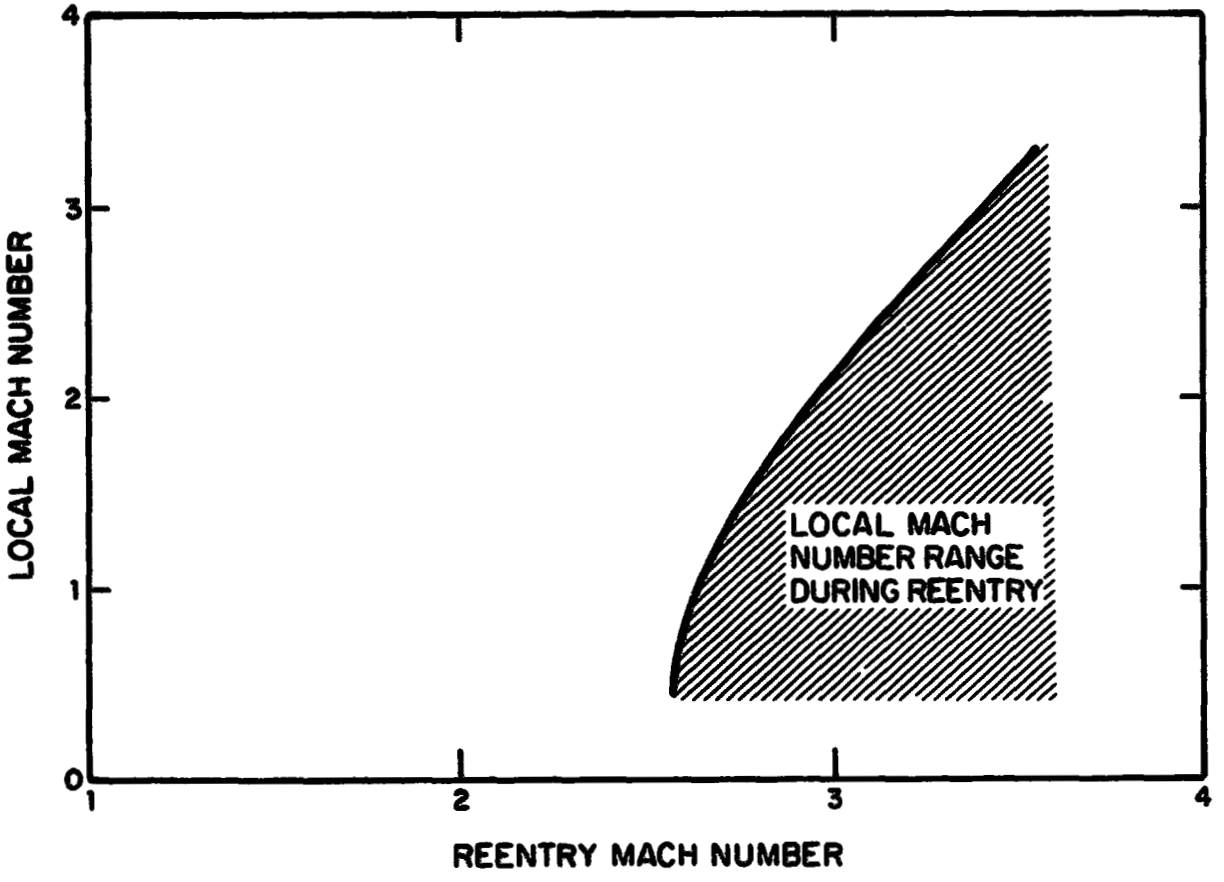

FIG. 10. PREDICTED LOCAL MACH NUMBER RANGE DURING REENTRY.

3. MODEL HEAT SHIELD OSCILLATIONS OBSERVED IN WIND TUNNEL TESTS

The characteristics of the heat shield oscillations observed during the AEDC tests are summarized in Table 1. Anticipating later developments, the corresponding results from flutter theory are also shown. The entries in this table indicate the ranges encountered for the quantities listed; no attempt has been made to distinguish between specific heat shield designs* or flow conditions (Mach number, angle of attack, tunnel density, etc.). No instrumentation intended specifically to measure the heat motion was installed on the model, so only the high speed film provides any specific information about the oscillations. These high speed films were not taken on all runs, but all films which display the oscillations show a regular wave motion starting at the portion of the annular heat shield nearest the stagnation point, and progressing around both sides of the annulus in the direction of air flow. The wave motion is symmetric about the diameter containing the stagnation point, with pairs of waves moving around the annulus from the stagnation point and meeting one another 180° from their point of origin. No reflected waves were discernible.

TABLE 1. MODEL HEAT OSCILLATIONS

	Measured	Flutter Theory
Wavespeed	152-178 cm/sec	150-760 cm/sec
Wavelength	4-12 cm	7-37 cm
Frequency	120-250 Hz	50-800 Hz
Amplitude	1.2 cm (approximately)	---

*Heat shields of three different materials and area mass densities were tested.

No forced-response phenomena known to the authors can explain this behavior. Even if a source of excitation at a single frequency were present in the flow, traveling waves would not be indicated unless the disturbance was limited to one region of the heat shield (specifically, the region from which the waves originated), or the disturbance itself were convected around the annulus with the observed speed of the waves in the heat shield. Note that the speed of the waves is considerably less than the fluid flow velocity which is on the order of 2500 cm/sec. Thus, the waves are not likely to be a passive response to a vortex or other disturbance convected with the flow.

On the other hand, the flutter theory presented in Sec. 4 predicts the following features of the motion observed in the wind tunnel tests:

(1) The basic wave-like character of the oscillations;
(2) Frequencies and wavelengths which are in fair quantitative agreement with experiment; and
(3) Good agreement with experiment as to the range of angles of attack at which the aeroelastic response is most severe.

Two additional points of agreement should be mentioned here. Although no attempt has been made to predict the amplitude of the heat shield oscillation, nonlinear panel flutter theory predicts that it should be on the order of the sag radius (Dowell, 1970). The sag radius of the model heat shields was R = 1.14 cm (0.45 in), which is roughly the amplitude of the oscillations seen in the films. Nonlinear flutter theory also predicts that a static pressure differential should reduce the amplitude of the response when the pressure is higher on the concave side of the heat shield, and increase it when the pressure is higher

on the convex side (Dowell, 1969 and 1970). Detailed calculations of the effect of a pressure differential are discussed in Sec. 4; here we mention only that one test run in which the pressure within the cavity behind the heat shield was greater than that outside produced violent oscillations and immediate failure of the heat shield.

The success of the flutter theory in predicting the basic features of the heat shield oscillations and the flow conditions under which they occur lead us to conclude that the oscillations were caused by aeroelastic flutter, rather than some forced response phenomenon.

4. HEAT SHIELD FLUTTER: BASIC THEORY AND APPLICATION TO 3% SCALE MODELS

In this section, we present basic theoretical results for heat shield flutter and discuss their application to the 3% scale heat shields used in the AEDC tests. Two separate theories are presented, one for low supersonic speeds and another for high supersonic speeds, because of basic differences in the parametric dependence of the aeroelastic response in these two flow regimes. The fundamental difference between the two theories is the method by which the aerodynamic loads on the oscillating heat shield are calculated. The simplified piston theory expression used in the high supersonic theory is usually considered to be acceptable for local Mach numbers greater than 1.5 or 2.0 (see Dixon [1966] or Dowell [1972]). In this report, we have chosen $M \div 1.5$ as the division between the two regimes. Further discussion of this point is provided in Sec. 4.3.

4.1 Prediction of Aeroelastic Loads

Under most test conditions, the oscillations encountered during the AEDC tests did not cause immediate failure of the heat shields. Similar oscillations in the full scale heat shield might also be acceptable, if it could be ascertained that they would not cause premature failure of the heat shield or nearby components during reentry. This approach would require that stresses and anchorage loads caused by flutter be determined with an acceptable level of confidence. The relevant theory is inherently nonlinear (Dowell, 1970), and requires lengthy numerical computations to treat even simple structural configurations (such as, for example, a rectangular homogeneous elastic plate with no applied structural loads). A recent attempt to compute *stresses* in a fluttering panel exposed to in-plane loads and a static pressure differential met with limited success

(Ventres and Kang, 1973). In our opinion, predicting aeroelastic loads *by theory alone* is beyond the state of the art. Therefore, we have limited our attention to predicting the onset of flutter, with the ultimate objective of using theory and experiment* to design a heat shield that will not flutter during reentry.

4.2 Low Supersonic Theory

The high speed films taken during the AEDC tests show waves progressing around the circumference of the annular heat shield. The wavelength of these waves is comparable to the width of the annulus (more precisely, the difference between the inner and outer radii). Since the wavelength is much smaller than either the semi-circumference or the mean radius of the heat shield, we have simplified the geometry for analytical purposes by "straightening out" the heat shield. That is, the aeroelastic model is not an annulus but an infinitely long panel having the same width as the annulus. The airflow is assumed to be parallel to the side edges of this infinite panel, as shown in Fig. 11.

To justify this flutter model, a series of companion calculations were made for a set of aluminum panels of various geometries. The quantity calculated in all cases is the thickness required of a homogeneous aluminum plate having the same *width* as the full scale SRB heat shield, so as to prevent flutter during reentry. The results are summarized in Table 2. They demonstrate the following points:

(1) The thickness required to prevent flutter is greater when the flow is circumferential.

---

*Recommended tests are discussed in Sec. 6.

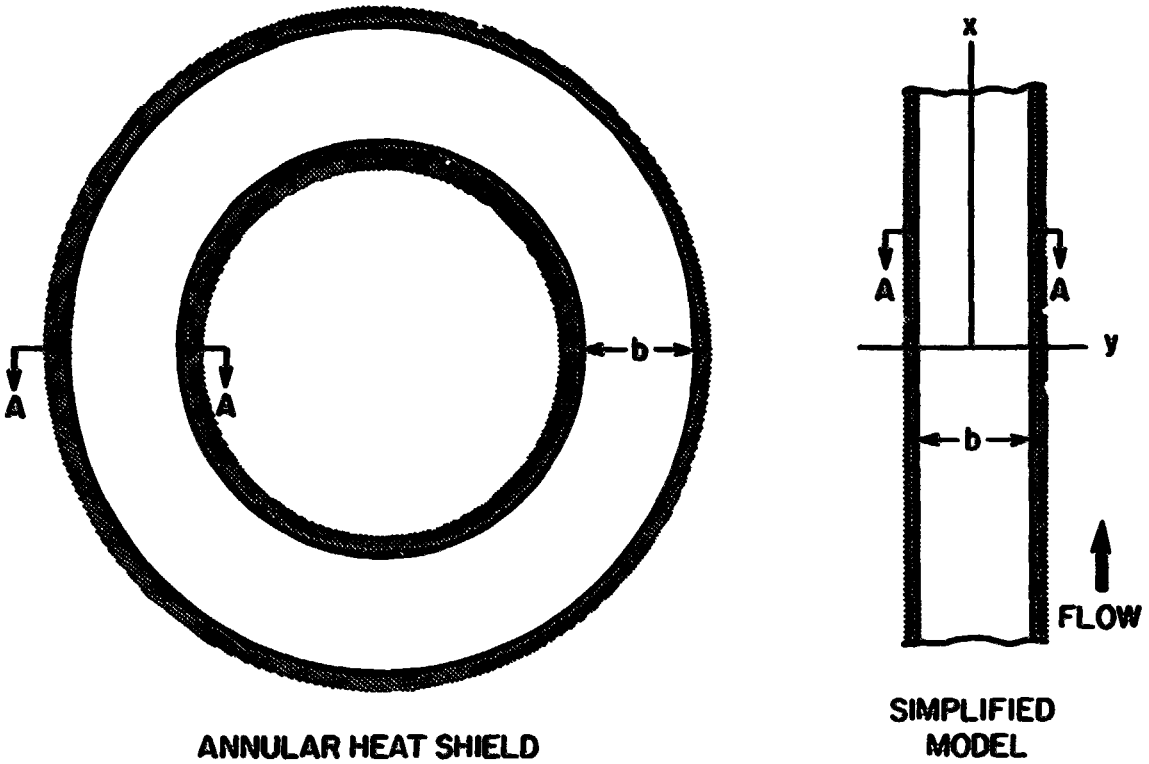

FIG. 11. SCHEMATIC DRAWING OF ANNULAR HEAT SHIELD AND THE SIMPLIFIED GEOMETRICAL MODEL

TABLE 2. THICKNESS REQUIRED TO PREVENT FLUTTER OF A FULL SCALE HEAT SHIELD CONSISTING OF A FLAT ALUMINUM PLATE 76.2 cm (30 in) WIDE: TEST OF ASSUMPTIONS ON CRITICAL DIRECTION OF FLOW AND LENGTH OF EQUIVALENT STRAIGHTENED HEAT SHIELD. LOCAL MACH NUMBER = 1.3.

	Direction of Flow	
Plate Length	Lengthwise (Circumferential)	Across Width (Radial)
76.2 cm (30 in)	0.79 cm*	
∞	0.86 cm**	0.72 cm***

* From Fig. 2 of Dixon (1966). The mean semi-circumference of the full scale heat shield is 710 cm.

** Using present low supersonic traveling wave theory based on Dowell (1966).

*** From Dowell (1975). Assumes $q_{flutter} b^3/D = 25$.

(2) The effect of finite length in the direction of airflow is small, and in any event, assuming an infinitely long panel is conservative (i.e., requires a thicker plate to prevent flutter).

A schematic drawing of the annular heat shield and the straightened out approximation are shown in Fig. 11. The full scale heat shield is constructed so that the heat shield fabric forms a sag radius of 37.3 cm (14.7 in) between the nozzle anchorage ring and the aft skirt. The equivalent radius (at 3% scale) was formed into the model heat shields, and is shown in Fig. 11 as the sag radius R. This has been incorporated in the straightened model as cross-stream curvature of the same radius R.

The analysis that follows is basically an adaptation of the method devised by E.H. Dowell (1966) to treat the flutter of an infinitely long flat plate. His analysis has been extended to include cross-stream curvature and a static pressure differential (unequal pressures on the inner and outer surfaces of the heat shield).

The linearized equations of motion of a plate curved in one direction are:

$$D\nabla^4 w + \frac{1}{R}\frac{\partial^2 \psi}{\partial x^2} - N_x \frac{\partial^2 w}{\partial x^2} - N_y \frac{\partial^2 w}{\partial y^2} + m\frac{\partial^2 w}{\partial t^2} + p = 0 \qquad (1)$$

$$\nabla^4 \psi - \frac{Eh}{R}\frac{\partial^2 w}{\partial x^2} = 0 \qquad (2)$$

As depicted in Fig. 11, the x-axis extends along the infinite dimension of the plate, whose side edges are located at $y = \pm b/2$. The airflow is in the direction of increasing x. Refer to the List of Symbols for other definitions.

In Eq. (1), N_x and N_y are the middle surface stress resultants caused by the static pressure differential Δp. Since the sag radius R is roughly equal to b/2, the heat shield takes on the shape of a half-torus (bisected at the meridian plane). Therefore, the stresses in the heat shield due to the pressure differential will be the same as those in an internally pressurized torus (or inner tube), which are approximately*

$$N_x = \frac{\Delta p R}{2}$$

$$N_y = \Delta p R \qquad (3)$$

The method of solution is to assume a traveling wave solution for the normal deflection w(x,y,t) and the Airy Stress function $\psi(x,y,t)$:**

$$w = \mathrm{Re}\left\{\hat{w}\ e^{i\alpha(ct-x)}\right\} \cos\left(\frac{\pi y}{b}\right)$$

$$\psi = \mathrm{Re}\left\{\hat{\psi}\ e^{i\alpha(ct-x)}\right\} \cos\left(\frac{\pi y}{b}\right) \qquad (4)$$

*Exact formulas are provided in Dym (1974). The expressions given above become exact when the ratio of the sag radius R to the circumference of the heat shield vanishes.

**These expressions imply simply supported boundary conditions on w and stress-free boundary conditions on ψ.

These expressions are substituted into Eq. (2) to determine $\hat{\psi}$ in terms of $\hat{w}$:

$$\hat{\psi} = -\frac{Eh}{R} \frac{\alpha^2 \hat{w}}{\left(\alpha^2 + \frac{\pi^2}{b^2}\right)^2} \tag{5}$$

If we now substitute Eq. (4) into Eq. (1), multiply by $\cos(\pi y/b)$ and integrate from $y = -b/2$ to $y = +b/2$, and finally use Eq. (5) to eliminate $\hat{\psi}$, we obtain

$$\left\{ D\left(\alpha^2 + \frac{\pi^2}{b^2}\right)^2 + \frac{Eh}{R^2} \frac{\alpha^4}{\left(\alpha^2 + \frac{\pi^2}{b^2}\right)^2} + N_x \alpha^2 + N_y \frac{\pi^2}{b^2} \right.$$

$$\left. - mc^2\alpha^2 \right\} \frac{b}{2} \hat{w} e^{i\alpha(ct-x)} + \int_{-b/2}^{b/2} p \cos\left(\frac{\pi y}{b}\right) dy = 0 \tag{6}$$

The last term in Eq. (5) contains an integral of the pressure p caused by the travelling wave deflection w. In his investigation of the flutter of infinitely long flat plates, Dowell (1966) reduced this expression to a function $F(\eta)$ of a single variable η, which he evaluated numerically:

$$\int_{-b/2}^{+b/2} p \cos(\pi y/b) dy = -\rho\alpha^2 (U - c)^2 \frac{b^2}{2} F(\eta) \cdot \hat{w} e^{i\alpha(ct-x)} \tag{7}$$

where

$$\eta \equiv \left(\frac{\pi b}{\ell}\right)^2 \left[1 - M^2 \left(1 - \frac{c}{U}\right)^2\right] \tag{8}$$

The function $F(\eta)$ is defined in Dowell (1966) and is displayed graphically in Fig. 2 of Dowell (1964). Equation (7) has been used for the aerodynamic pressure on the heat shield. This amounts to assuming that the relation between the heat shield motion and the resulting pressure is not substantially changed by the cross-stream curvature (heat shield sag).

If Eq. (7) is substituted into Eq. (6), we obtain an implicit relationship between the wavespeed c, the wavelength $\ell \equiv 2\pi/\alpha$, and the flow velocity U. This equation is written out below in dimensionless form:

$$\frac{1}{4}\left(\frac{\ell}{2b} + \frac{2b}{\ell}\right)^2 + 4\Gamma\left(\frac{\ell}{2b} + \frac{2b}{\ell}\right)^{-2}$$

$$+ \frac{\Delta p R b^2}{4\pi^2 D}\left[\frac{1}{2} + \left(\frac{\ell}{2b}\right)^2\right] - c^{*2} - \mu\left(U^* - c^*\right)^2 F(\eta) = 0 \tag{9}$$

The following notation has been introduced

$$\mu \equiv \rho b/m$$

$$\Gamma \equiv Ehb^4/(2\pi)^4 R^2 D \tag{10}$$

$$c_o \equiv 2\pi \left(D/mb^2\right)^{1/2}$$

$$c^* \equiv c/c_o$$

$$U^* \equiv U/c_o \qquad (11)$$

When U^* or μ is zero, Eq. (9) has two real solutions for the dimensionless wavespeed c^*. Above a certain value of U^*, however, the wavespeeds are complex, and one of the two corresponds to unstable motion, that is, waves that grow in amplitude. The value of U^* at which c^* becomes complex depends on the normalized wavelength $\ell/2b$; the *smallest* value of U^* is the one that is physically significant, since it corresponds to the initial appearance of instability. This value of U^* is denoted by U^*_{cr}, and is called the critical or flutter velocity. The corresponding values of c^* and $\ell/2b$ are denoted by c^*_{cr} and $(\ell/2b)_{cr}$. These are the critical or flutter wavespeed and wavelength, respectively.

In Figs. 3, 6 and 7 of Dowell (1966), c^*_{cr}, $(\ell/2b)_{cr}$ and U^*_{cr} are displayed graphically *for a flat plate* as functions of Mach number M and mass ratio μ:

$$c^*_{cr} = c^*_{cr}(\mu,M)$$

$$(\ell/2b)_{cr} = (\ell/2b)_{cr}\,(\mu,M)$$

$$U^*_{cr} = U^*_{cr}\,(\mu,M)$$

For a flat plate with no pressure differential, Dowell showed that the critical wavelength is closely approximated by the value which gives the minimum wavespeed in a vacuum ($\mu = 0$). Setting $\mu = \Delta p = \Gamma = 0$ in Eq. (9), we obtain, for the *in vacuo* wavespeed of a flat plate,

$$|c^*| = \frac{1}{2}\left(\frac{\ell}{2b} + \frac{2b}{\ell}\right)$$

Inspection of this equation shows that the minimum wavespeed is $|c^*_{min}| = 1$ when $\ell/2b = 1$. As shown in Fig. 6 of Dowell (1966), $(\ell/2b)_{cr} \doteq 1$ for any μ and M, and especially for $M \geq 1$ and $\mu << 1$. Thus, Dowell's results for $U^*_{cr}(\mu,M)$ and $c^*_{cr}(\mu,M)$ may be *generalized* to apply to a curved plate with a static pressure differential by interpreting them as U^*_{cr}/c_{min} and c^*_{cr}/c_{min}, respectively. Implicit in this generalization is the assumption that $F(\eta)$ can be treated as a constant in Eq. (9). Fortunately, $F(\eta)$ does not vary rapidly with the parameters of interest, i.e., μ, M, and $\ell/2b$.

As a result of this approximation, Figs. 3 and 7 of Dowell (1966) may be used directly to obtain U^*_{cr}/c_{min} and c^*_{cr}/c_{min} for a curved plate exposed to a static pressure differential. The flutter wavelength is assumed to be the minimum wavespeed in a vacuum, and *the influence of the pressure differential and the cross-stream curvature on the flutter velocity is determined entirely by their effect on the minimum wavespeed.*

It remains, therefore, to calculate the minimum wavespeed in a vacuum. This is done by setting $\mu = 0$ in Eq. (9), and solving for c^*:

$$c^* = \left\{ \frac{1}{4}\left(\frac{\ell}{2b} + \frac{2b}{\ell}\right)^2 + 4\Gamma\left(\frac{\ell}{2b} + \frac{2b}{\ell}\right)^{-2} + \frac{\Delta p R b^2}{4\pi^2 D}\left[\frac{1}{2} + \left(\frac{\ell}{2b}\right)^2\right]\right\}^{1/2} \qquad (12)$$

The dimensional wavespeed $c = c_o c^*$ obtained from this equation is shown plotted in Fig. 12, using the following values for the dimensions and the mechanical properties of the heat shield:

$$h = 0.025 \text{ cm } (0.01 \text{ in})$$

$$b = 2.29 \text{ cm } (0.9 \text{ in})$$

$$\sqrt{Eh/m} = 305. \text{ m/s } (1000 \text{ ft/sec})$$

These values were selected as being representative of the several heat shields used in the AEDC tests. They were obtained from data supplied by NASA MSFC (see Appendix A). In calculating c_o and Γ, we assumed that the plate bending stiffness D could be approximated by its value for a homogeneous elastic plate,

$$D = \frac{Eh^3}{12(1-\nu^2)}$$

in spite of the heat shields' non-homogeneous construction.* This approximation was required because no independent measurement of D was available.

In Fig. 12, the *in vacuo* wavespeed is shown as a function of $\ell/2b$ for several values of Δp. When $\Delta p = 0$, there are two values of $\ell/2b$ that provide the same minimum wavespeed. Of these, the longer of the two wavelengths is found to result in the lowest critical velocity U^*_{cr}, because $F(\eta)$ is a monotonically decreasing function of η, and larger $\ell/2b$ means *smaller* η (see Eq. [8]) and thus *larger* $F(\eta)$ in Eq. (9). By the same reasoning,

*Some of the heat shields were constructed of nylon mesh impregnated with rubber.

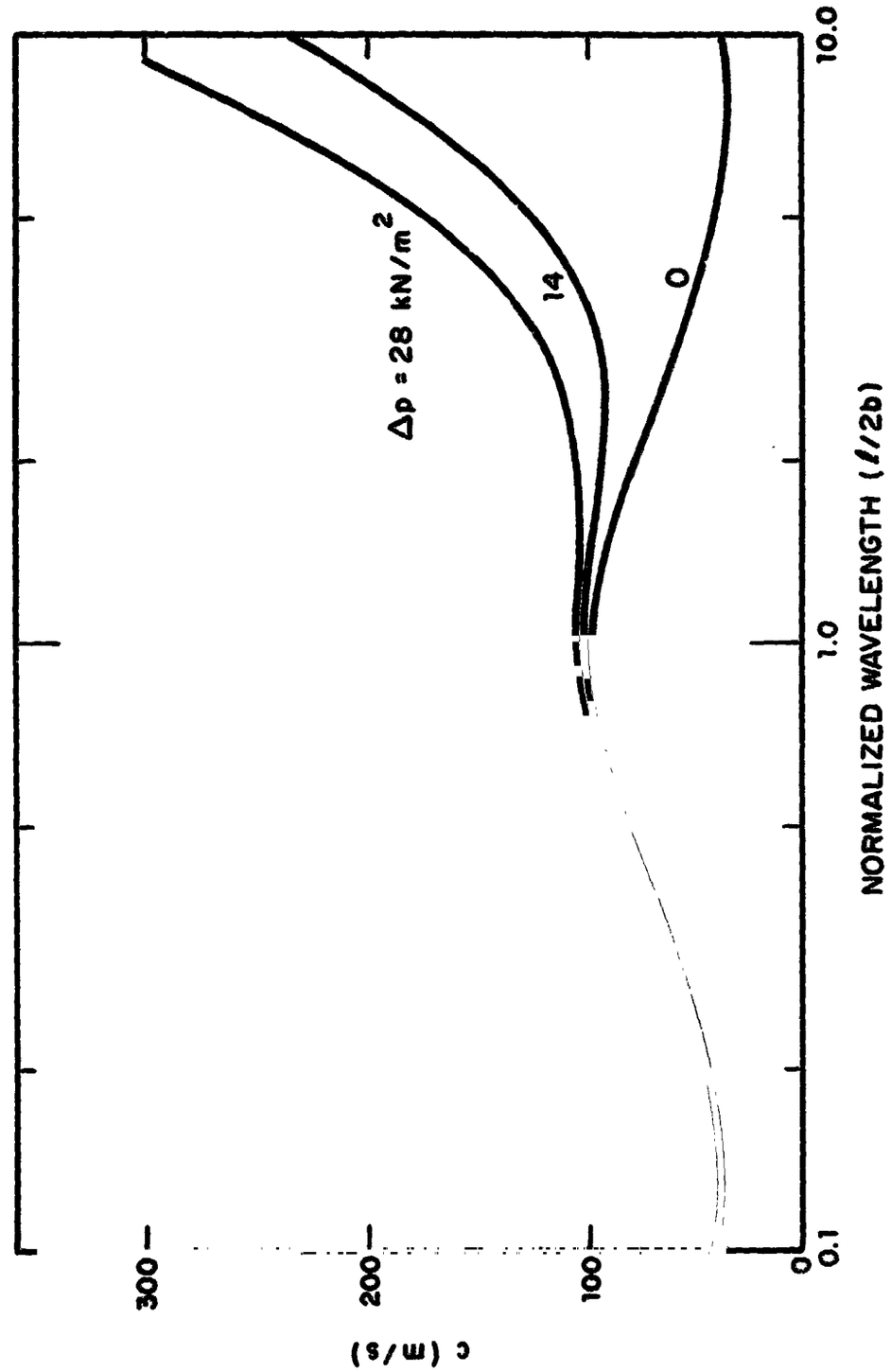

FIG. 12. *IN-VACUO* WAVESPEED IN 3% SCALE MODEL HEAT SHIELD

the local minima in the wavespeed c in Fig. 12 for which $\ell/2b > 1$ remain critical as Δp is increased. The critical wavelength $(\ell/2b)_{cr}$ is displayed in Fig. 13 as a function of Δp. Note that increasing Δp causes a rapid *decrease* in the critical wavelength, and an *increase* in the critical wavespeed.

The flutter velocities calculated as described above are displayed in Fig. 14. These flutter boundaries are shown *vs.* Mach number for several values of Δp. The unstable region in the figure is to the right and above these curves. Also shown in the same figure is the air flow velocity in the wind tunnel, which operated at a constant stagnation temperature of 311°K (560°R). The Mach number on the horizontal axis is the local Mach number over the face of the heat shield, not the freestream or test section Mach number. Recall that the local Mach number depends on the angle of attack; as the angle of attack increases, the local Mach number drops from M_∞ toward 1 (see Fig. 8). Thus, at low angle of attack the flow velocity is high; as the angle of attack increases, the flow velocity decreases, following the wind tunnel curve in Fig. 14 from right to left in the direction of decreasing local Mach number. Eventually, a stability boundary is crossed and flutter is *suppressed.* The local Mach number at which this occurs is shown in Fig. 15, which is merely a cross-plot of Fig. 14. The angle of attack at which the stability boundary is crossed will, of course, depend on the free stream Mach number in accordance with Fig. 8.

The AEDC tests were conducted at $M_\infty = 2.75$ and 3.5. Therefore, Fig. 14 implies that for $\Delta p \leq 13{,}790$ N/m^2 (2 psi), flutter always occurred at low angles of attack, but was eventually suppressed at higher angles. As we shall see, this conclusion will be altered when the stability boundaries in Fig. 14 have been modified to incorporate the high Mach number flutter theory.

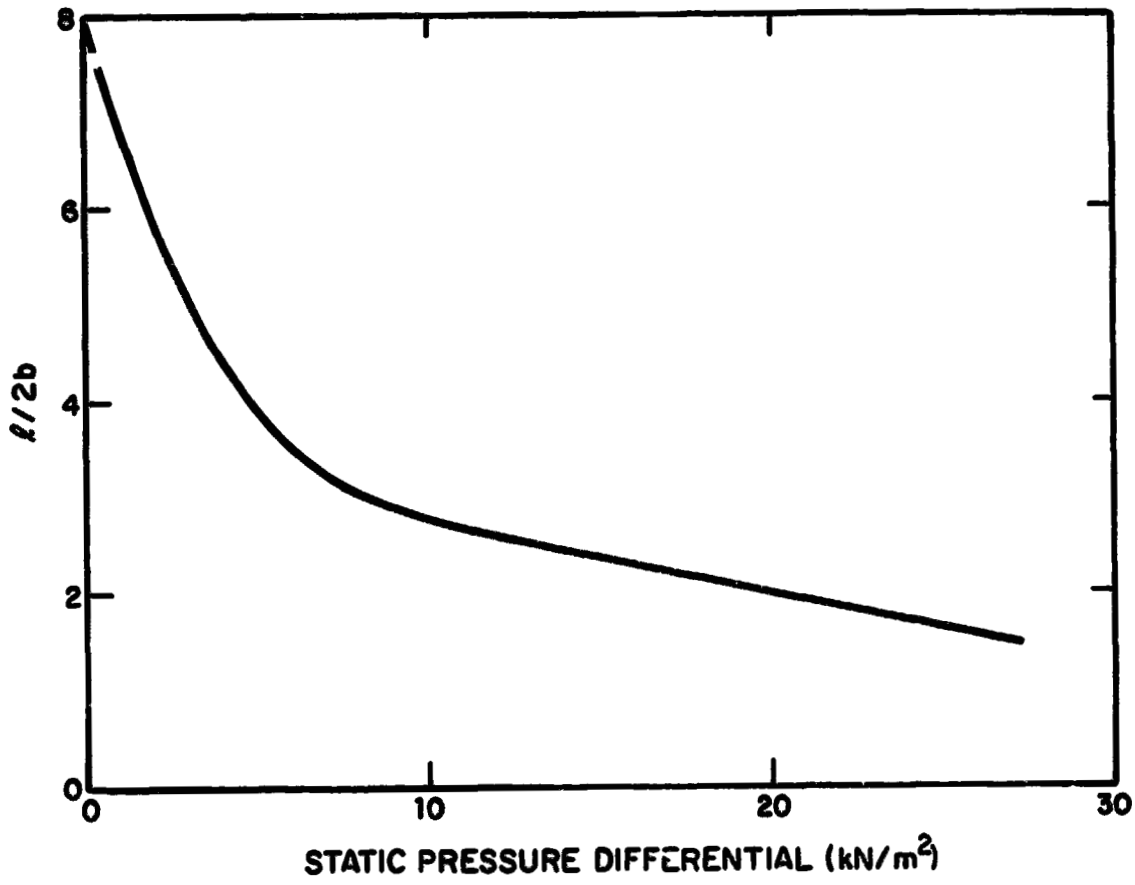

FIG. 13. CRITICAL WAVELENGTH VS PRESSURE DIFFERENTIAL

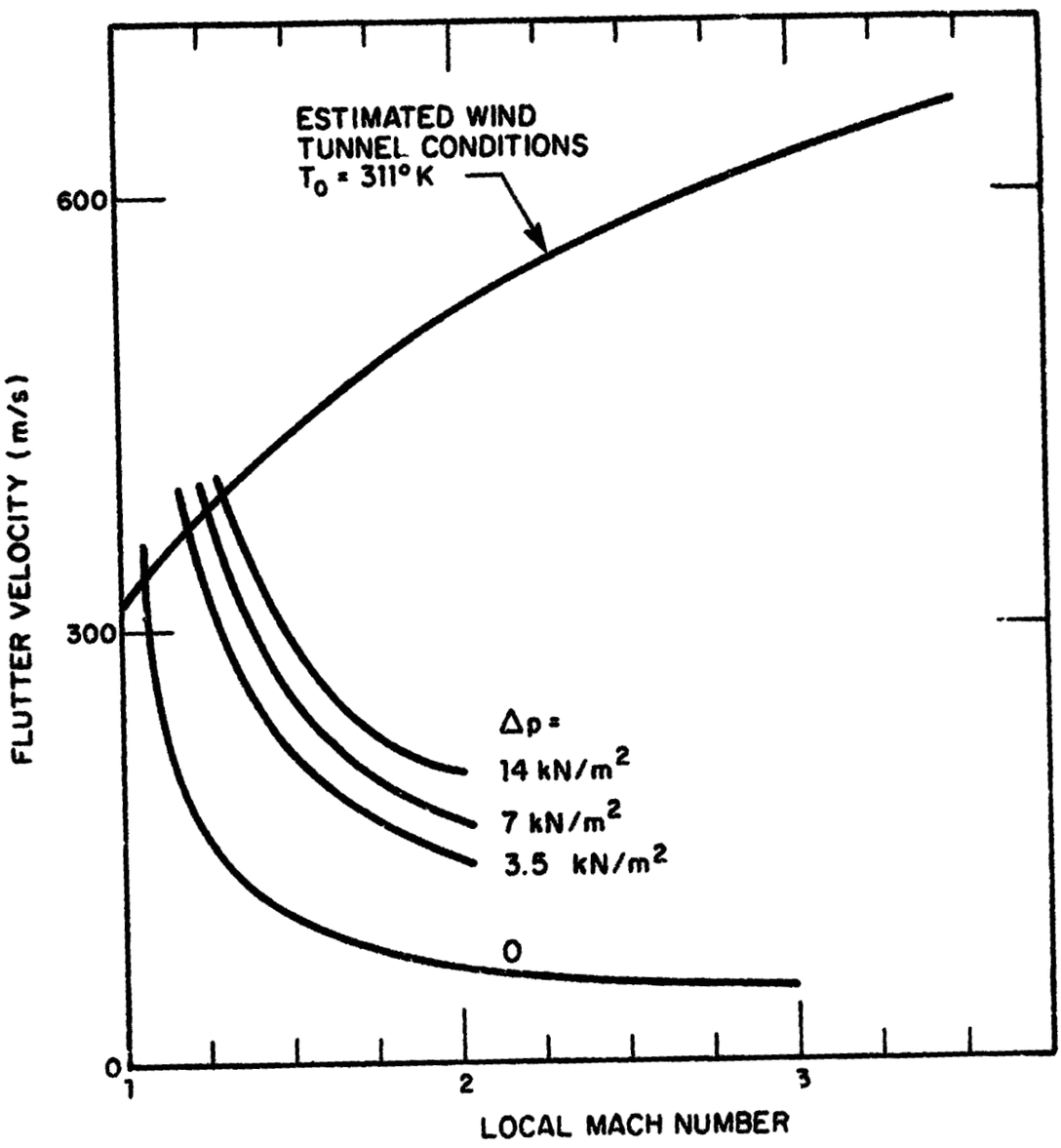

FIG. 14. STABILITY BOUNDARIES FOR 3% SCALE HEAT SHIELDS

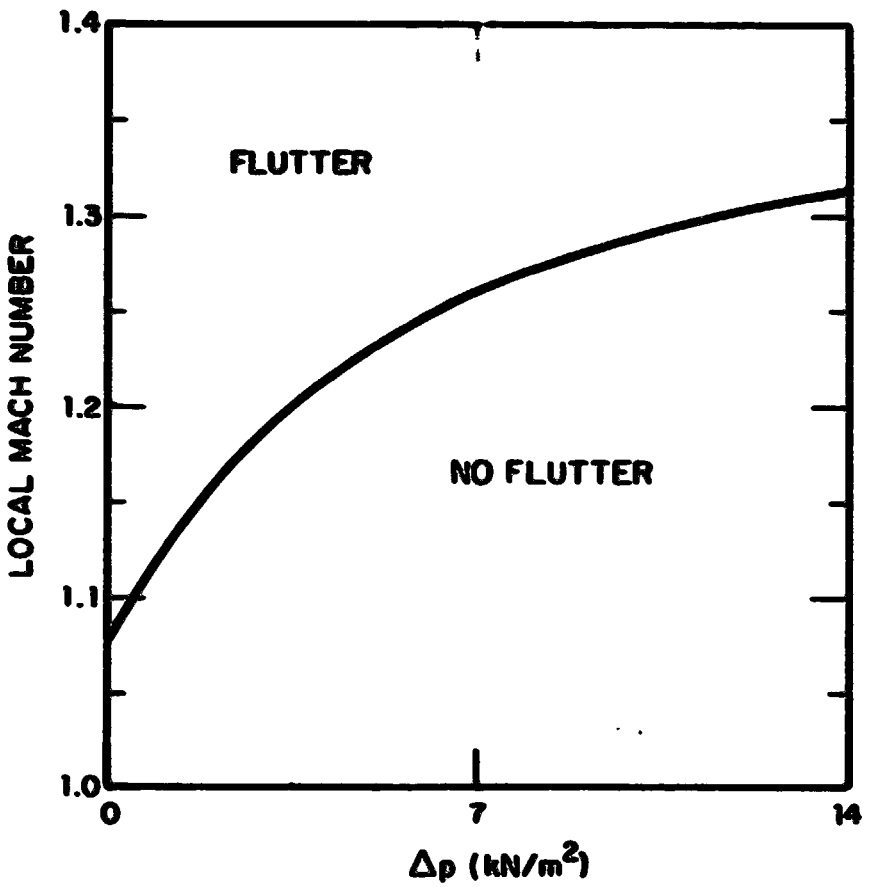

FIG. 15. STABILITY BOUNDARY: LOCAL MACH NUMBER VS PRESSURE DIFFERENTIAL

Critical wavespeeds and frequencies are shown in Figs. 16 and 17 for $\Delta p = 0$ and 13,790 N/m^2 (2 psi). The pressure differential Δp increases the critical wavespeed at any given Mach number by the same proportion that it increases the *in vacuo* wavespeed. The flutter frequency is given by

$$f = \frac{c_{cr}}{\ell_{cr}}$$

The pressure differential increases the critical wavespeed and at the same time decreases the critical wavelength (see Fig. 12); thus, the frequency is increased by a greater proportion than is the wavespeed.

4.3 High Supersonic Theory

For M > 1.5 or so the assumption of a traveling wave solution (Eqs. [4]) is no longer appropriate (Dowell and Ventres, 1970). However, a stability boundary based upon the use of piston theory aerodynamics and the assumption that the length of the plate in the streamwise direction is much greater than its width, can be derived from the theory presented by Dowell and Ventres (1970). This stability boundary was derived for rectangular plates, so we are retaining the concept of an equivalent straight heat shield as discussed previously.

The stability boundary is given below,

$$\frac{qb^3}{\beta D} = \frac{(2\pi^2)^{3/2}}{\pi^3} \left[1 + \frac{1}{2\pi^2} \left(\frac{\Delta p R b^2}{2D}\right)\right]^{3/2} \qquad (13)$$

where $\beta \equiv (M^2-1)^{1/2}$, and $q \equiv 1/2\ \rho U^2$ is the local dynamic pressure. Note that the stability boundary is defined in terms of the dynamic pressure rather than the velocity as it was at low supersonic speeds. Critical values of q/β calculated from this

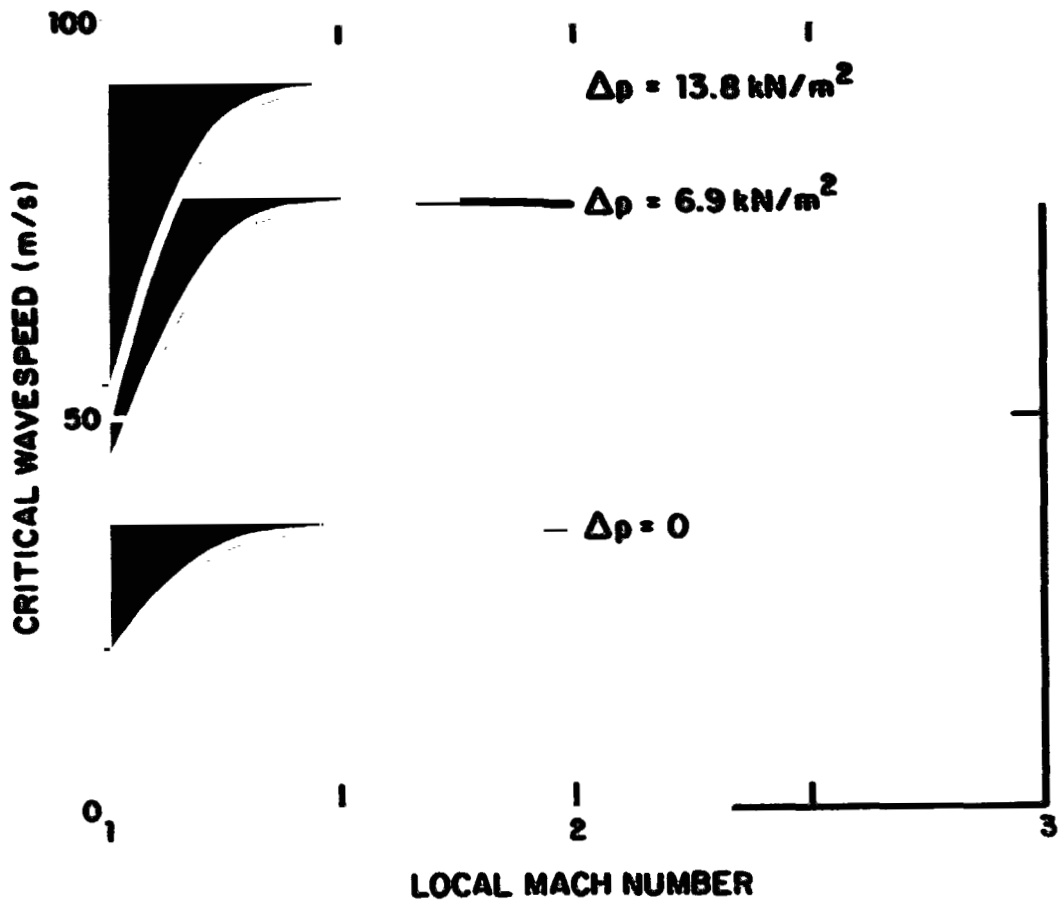

FIG. 16. CRITICAL WAVESPEED VS LOCAL MACH NUMBER FOR 3% SCALE HEAT SHIELDS

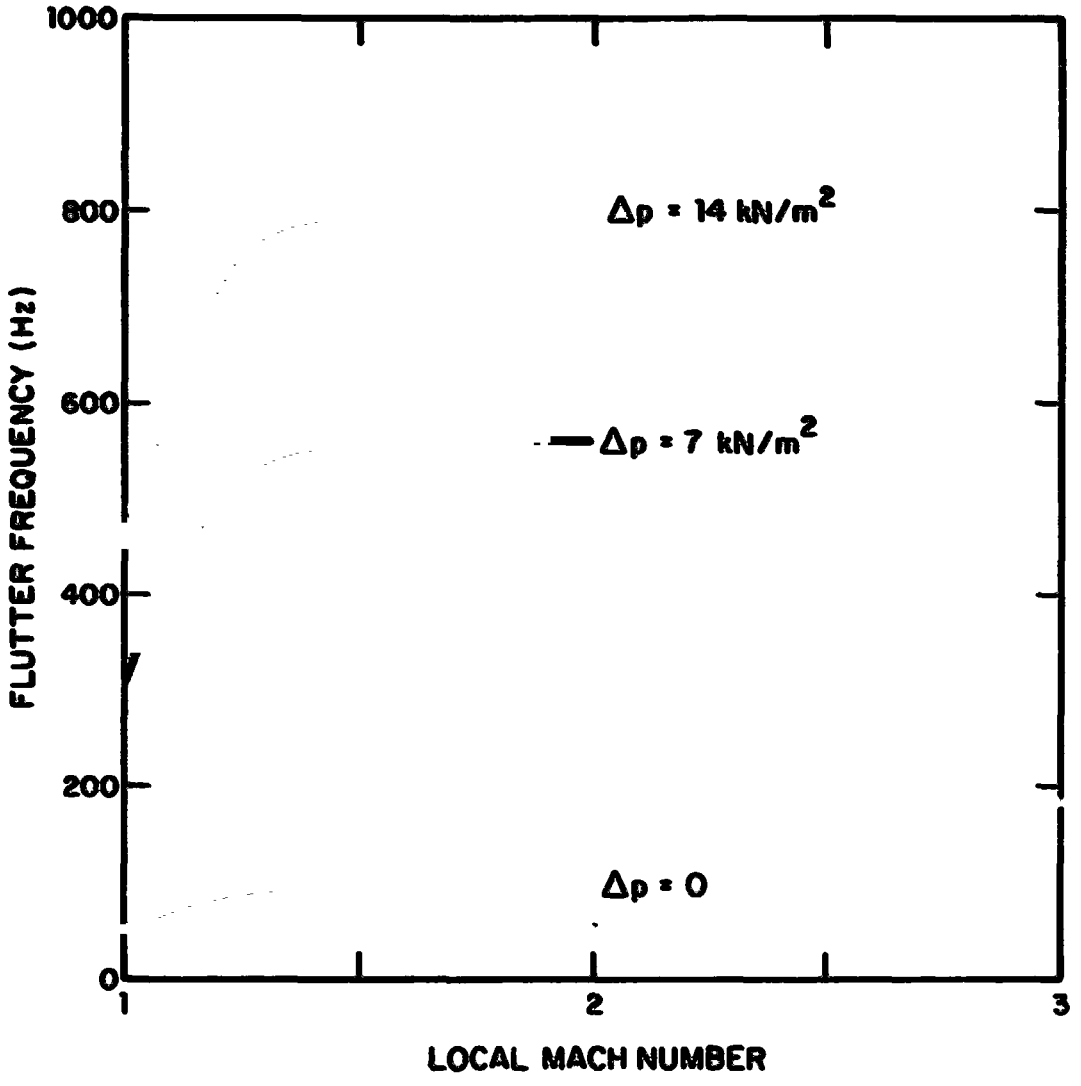

FIG. 17. CRITICAL WAVELENGTH VS LOCAL MACH NUMBER FOR 3% SCALE HEAT SHIELDS

equation for several values of Δp are shown in Table 3. The mechanical properties listed on page 30 were used for the computations.

TABLE 3. $(q/\beta)_{flutter}$ vs. Δp ($M \geq 1.5$)

Δp	$(q/\beta)_{flutter}$
0	0.139 kN/m² (.0201 psi)
7 kN/m² (1 psi)	7.93 kN/m² (1.15 psi)
13.8 kN/m² (2 psi)	13.9 kN/m² (3.08 psi)
27.6 kN/m² (4 psi)	58.5 kN/m² (8.49 psi)

In Figs. 18 and 19, stability boundaries for M_∞ = 2.75 and 3.5 are displayed along with the range of local q/β encountered at each angle of attack. The unstable regime is toward the top of each figure, i.e., $(q/\beta)_{local} > (q/\beta)_{flutter}$. During the tests, the tunnel dynamic pressure was varied at constant M_∞ by changing the tunnel total pressure p_o. The dashed curves in both figures are the values of q/β that correspond to the maximum and minimum tunnel stagnation pressures used at each test section Mach number. These dashed curves are terminated at the angle of attack where the local Mach number dropped to 1.5. Below this Mach number, or alternatively, above the corresponding angle of attack, the stability boundaries do not apply, and the low supersonic theory must be used instead.

Both figures show that flutter is suppressed by a pressure differential of 28 kN/m² (4 psi) at all tunnel stagnation pressures, except for a small range of angles near 120° at M_∞ = 3.5.

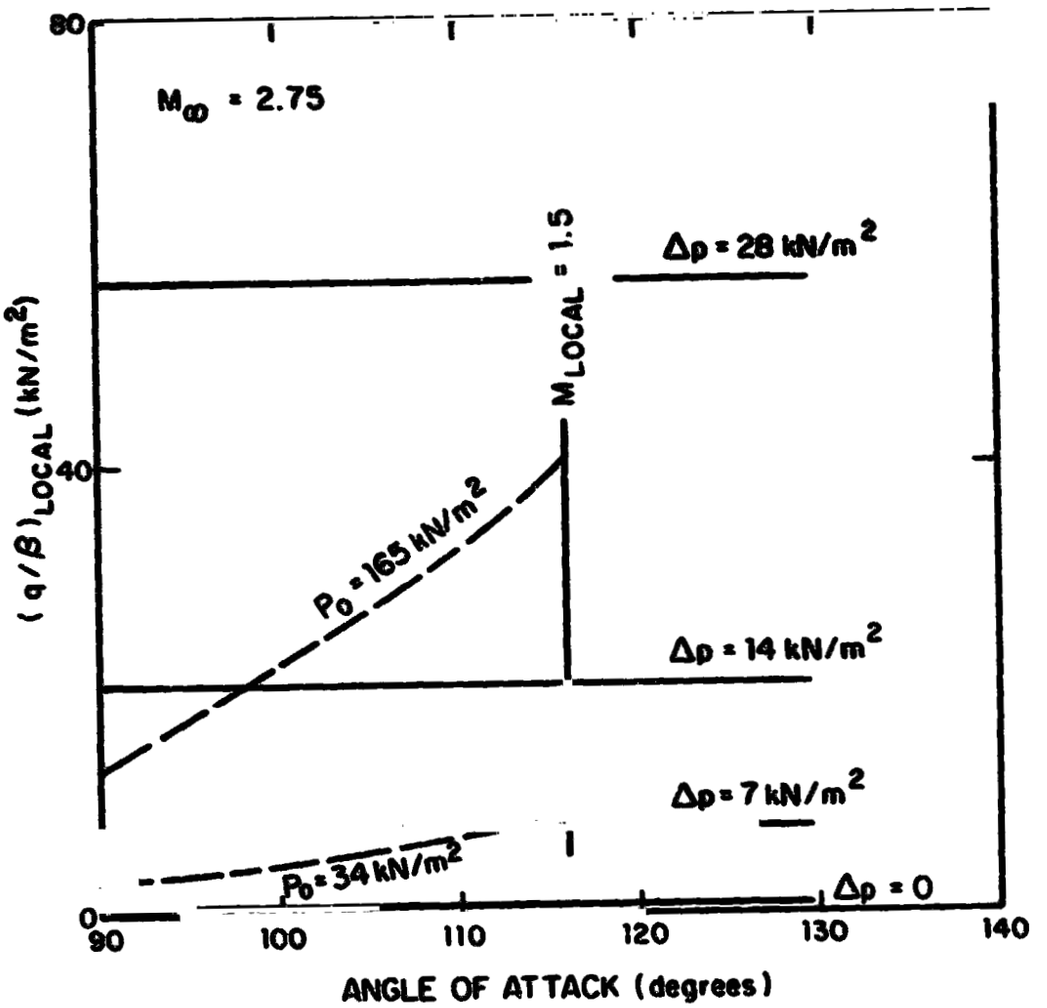

FIG. 18. FLUTTER DYNAMIC PRESSURE FOR 3% SCALE HEAT SHIELDS, M_∞ = 2.75

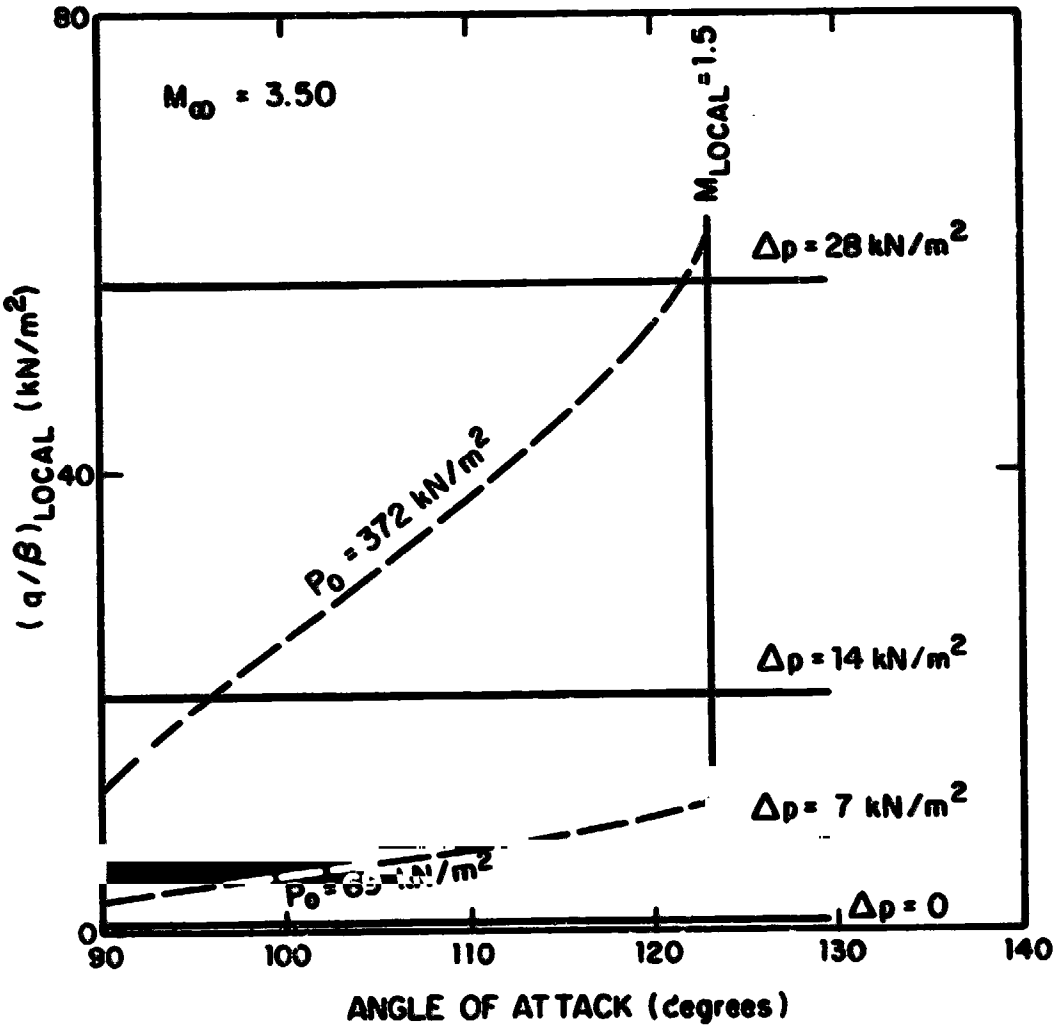

FIG. 19. FLUTTER DYNAMIC PRESSURE FOR 3% SCALE HEAT SHIELDS, M_∞ = 3.50

The stabilizing effect of Δp is much more pronounced at high Mach numbers than at the lower speeds.

In Figs. 20 and 21 are shown composite curves, for $M_\infty = 2.75$ and $M_\infty = 3.5$, which incorporate both the low and high Mach number stability boundaries. They are plotted as flutter velocity vs. local Mach number. Curves are shown for $\Delta p = 0$ and $\Delta p = 7$ kN/m^2 (1 psi). The stability boundaries for each value of Δp bifurcate at M = 1.5; as explained previously, above that Mach number flutter occurs at constant q/β rather than constant velocity. The dashed portions of each curve are *sketched* in to provide smooth transitions between the two Mach number regimes. Also shown in both figures is the wind tunnel flow velocity vs. local Mach number. Flutter is indicated whenever the wind tunnel curve lies above the appropriate stability boundary.

Each figure is for a specific test section Mach number; the local Mach number over the face of the heat shield varies as the angle of attack changes. Note that at both $M_\infty = 2.75$ and $M_\infty = 3.5$, a pressure differential of 7 kN/m^2 (1 psi) suppresses flutter over all but a very limited range of local Mach numbers when the tunnel is operated at reduced total pressure. Larger Δp's would have the same effect at higher tunnel total pressures. Since local Mach number is related to angle of attack (recall Fig. 8), flutter occurs over only a limited range of angle of attack as well. At both $M_\infty = 2.75$ and 3.5, flutter occurs when the local Mach number is between 1.3 and 2. From Fig. 8, the corresponding ranges of angle of attack are $107° < \alpha < 118°$ at $M_\infty = 2.75$, and $116° < \alpha < 126°$ at $M_\infty = 3.5$. Both of these ranges agree fairly well with the angles over which the highest fluctuating pressure levels were recorded in the AEDC tests. The noise spectra measured at these angles show a pronounced low frequency content (below 500 Hz) that can reasonably be attributed to the

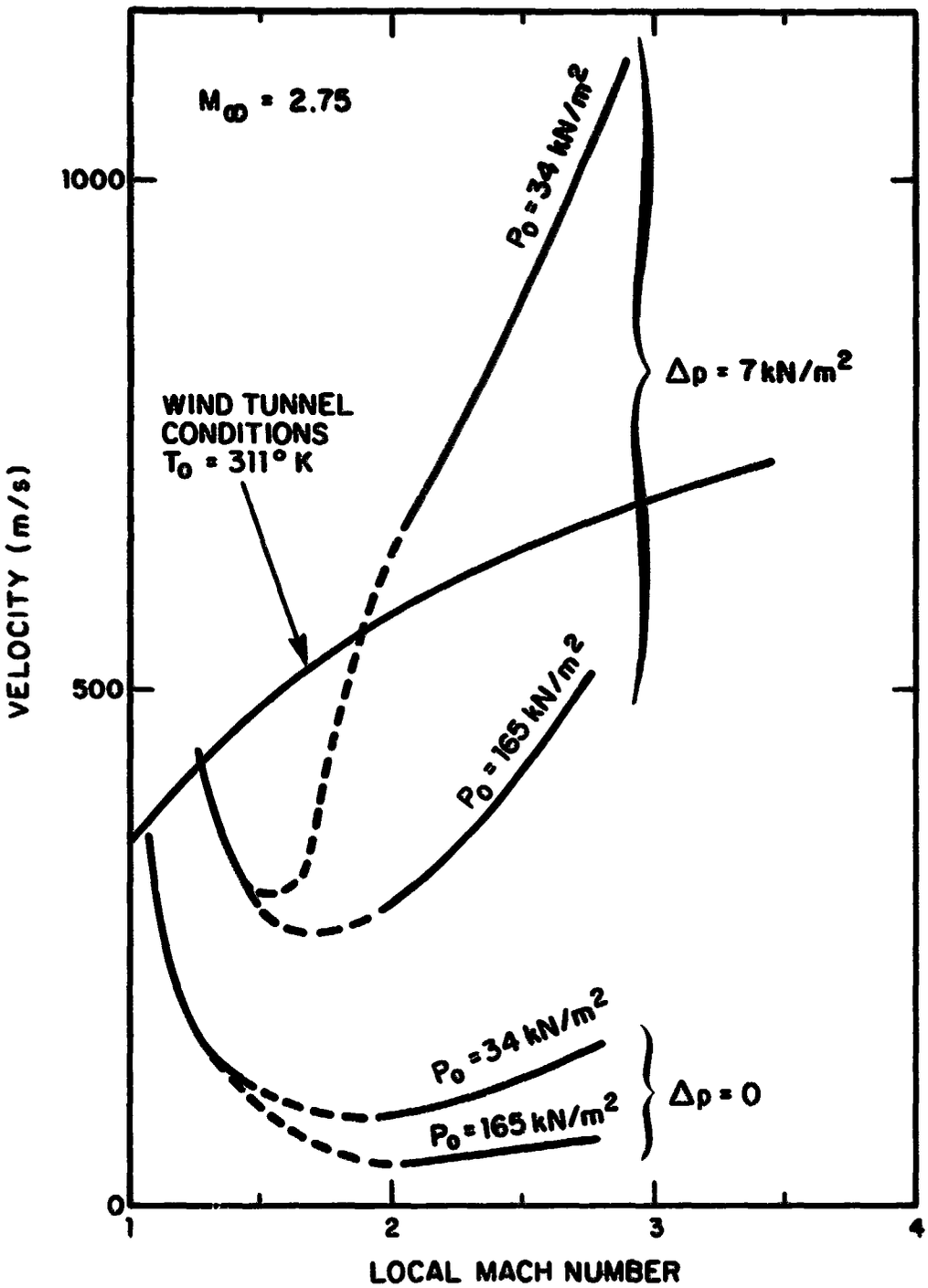

FIG. 20. COMPOSITE STABILITY BOUNDARIES FOR 3% SCALE HEAT SHIELDS, M_∞ = 2.75

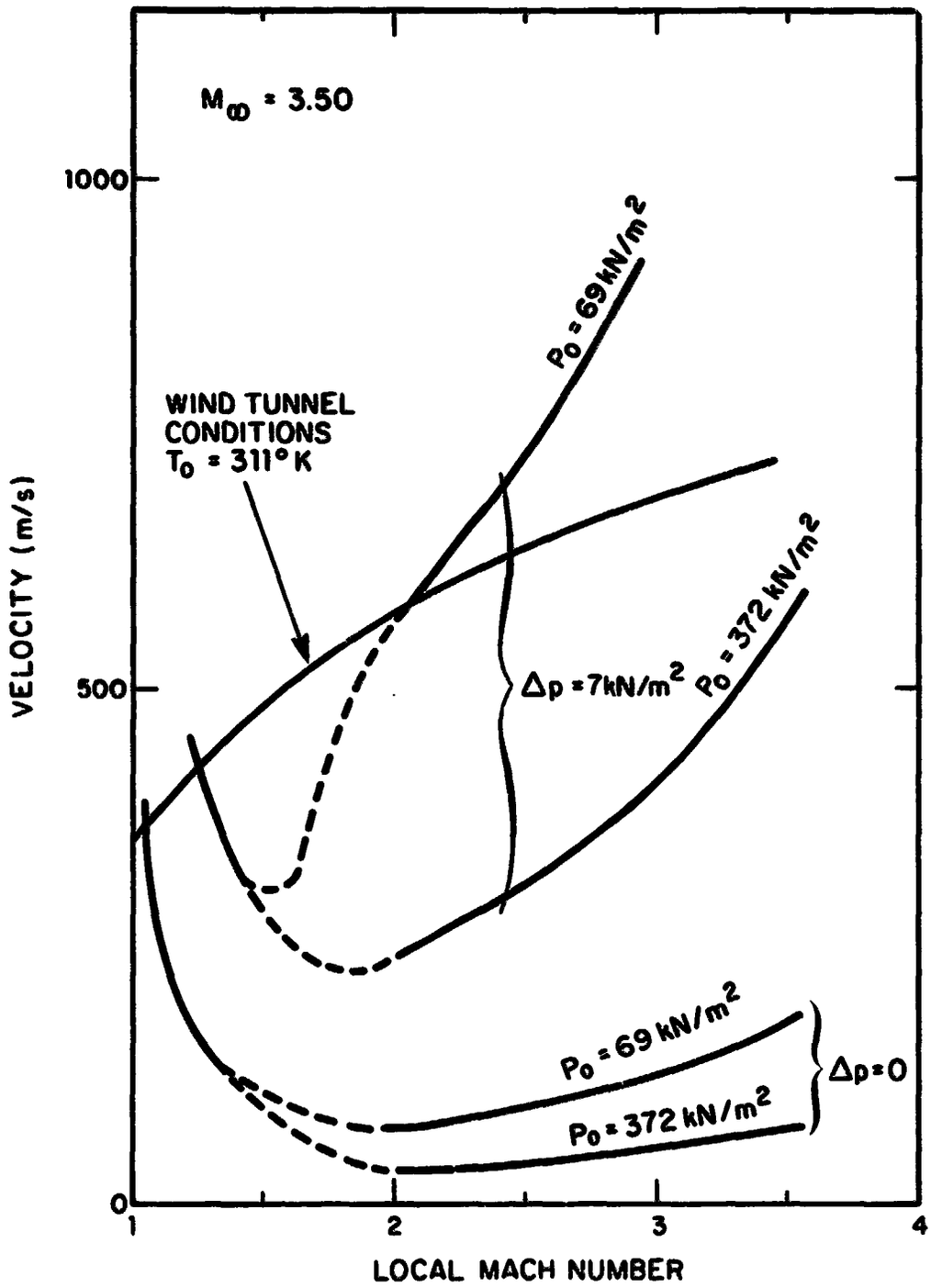

FIG. 21. COMPOSITE STABILITY BOUNDARIES FOR 3% SCALE HEAT SHIELDS, M_∞ = 3.50

heat shield oscillation frequency and its overtones. In this respect, therefore, the theory correlates well with the experiment.

The critical Mach number range, where flutter is most likely to occur, lies at the transition between the low and high supersonic regimes (the dashed portion of the flutter boundaries in Figs. 20 and 21). A single flutter theory, valid for all supersonic Mach numbers, would be therefore highly desirable. Such a theory was not attempted, however, because of the numerical complications involved. The simplified low and high Mach number theories presented in Sections 4.2 and 4.3 are adequate to explain the wind tunnel data and to provide guidance for improving the design of the full scale SRB heat shield.

5. FULL SCALE SRB HEAT SHIELD: REQUIREMENTS FOR FLUTTER PREVENTION AND PROPOSED DESIGN MODIFICATIONS

5.1 Present Heat Shield Design

The SRB heat shield consists of 24 segments laced together along the radial edges to form a complete annulus. The heat shield is attached to the nozzle on the inner perimeter and to the aft skirt on the outer perimeter. The segments are sized so that each assumes a sag radius of 37.3 cm (14.7 in).

The segments are made up of three layers of material, sewn together in a square quilt pattern. The outermost layer is heat resistant #581 Astroquartz woven cloth, and the inner layer is #1582 Fiberglass. Between these is sandwiched a layer of Fiberfrax insulation. Most of the strength of the heat shield derives from the inner and outer layers.

The surface mass density of the heat shield is about 1.88 kg/m^2 (0.012 $slugs/ft^2$). All other mechanical properties of the heat shield bearing on its aeroelastic stability are unknown.

For most purposes, the heat shield is a limp membrane-like structure. With regard to flutter however, its bending stiffness, however small, is of crucial importance.* The bending stiffness of a homogeneous elastic plate is related to the Young's Modulus and to the thickness h by the familiar formula $D = Eh^3/12(1-\nu^2)$. The heat shield, however, is built up of three different materials and because of its quilted construction, the thickness h is not constant. Thus, D must be determined by experiment.

*The bending stiffness D appears implicitly in Eq. (9), which determines the flutter velocity at low supersonic Mach numbers, and explicitly in Eq. (13), which determines the flutter dynamic pressure at hign supersonic Mach numbers.

Also significant with regard to flutter is the ratio between in-plane tension and in-plane strain. For a homogeneous plate this ratio is Eh. For the fabric heat shield, whereas the product Eh has the same physical significance, E and h are not separately defined. Eh also must be determined by experiment.

Because the bending stiffness of the full scale heat shield is unknown, we were not able to calculate flutter boundaries analogous to those presented in Sec. 3 for the model heat shields. Instead we have calculated, using the same theory, *the bending stiffness required to prevent flutter during reentry.* The purpose here is to establish whether or not the heat shield as presently conceived may reasonably be expected to have the required stiffness. The conclusion reached is that it cannot.

5.1.1 Stiffness Required to Prevent Flutter at Low Supersonic Speeds

In Fig. 22 is shown the minimum wavespeed *in vacuo* for the full scale heat shield. The parameter in the figure is the in-plane stiffness Eh. These curves were calculated from Eq. (12), using b = 76.2 cm (30 in.) and m = 1.88 kg/m^2 (0.012 slugs/ft^2). The in-plane stiffness increases the wavespeed by virtue of the added hoop stiffness due to the cross-stream curvature R. The increase in wavespeed is only 50% when Eh increases from 0 to 17500 kN/m (10^5 lb/in.).

The local flow velocity over the heat shield during reentry is displayed in Fig. 23 for several values of freestream or reentry Mach number. For all *local* Mach numbers, the highest *local* velocity is encountered when the reentry Mach number is 3.5. Assuming M_{local} = 1.5 (the highest Mach number at which the low Mach number theory is accurate), we obtain U = 640 m/sec (2100 ft/sec).

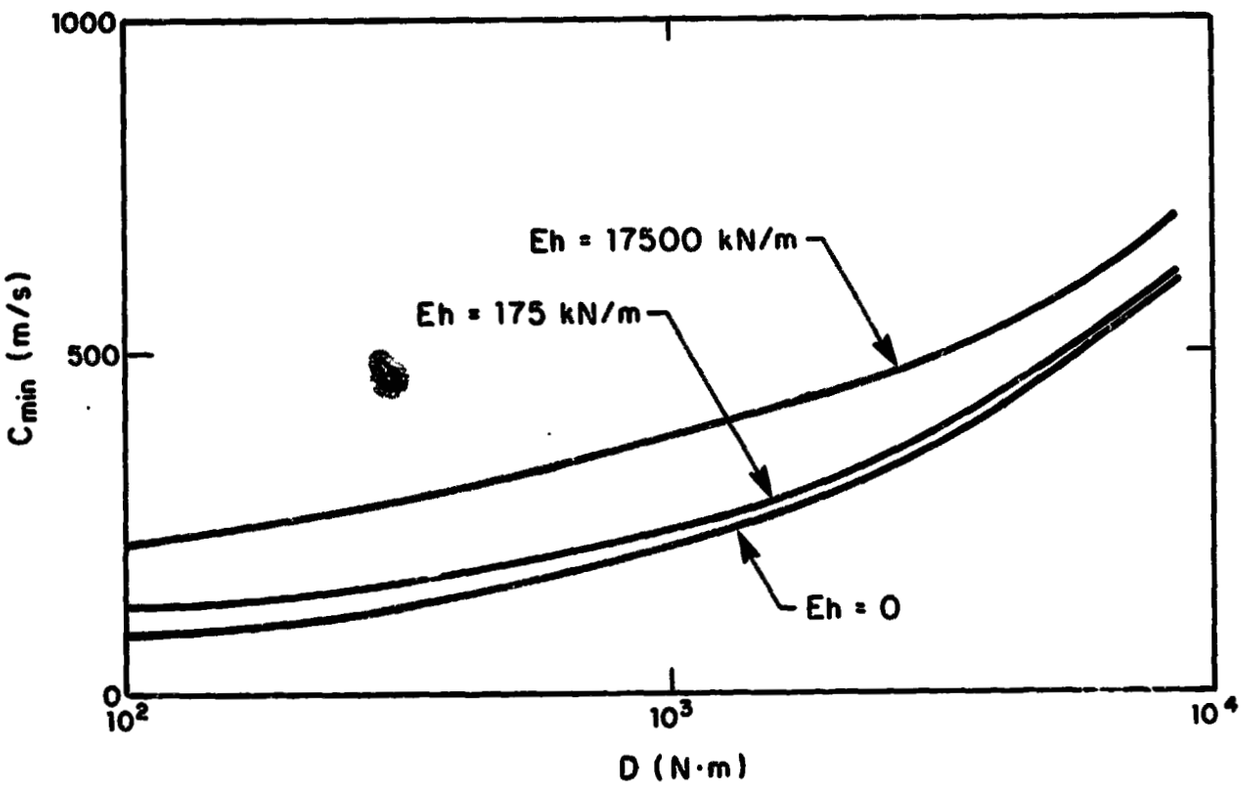

FIG. 22. *IN-VACUO* WAVESPEED IN SRB HEAT SHIELD VS BENDING STIFFNESS

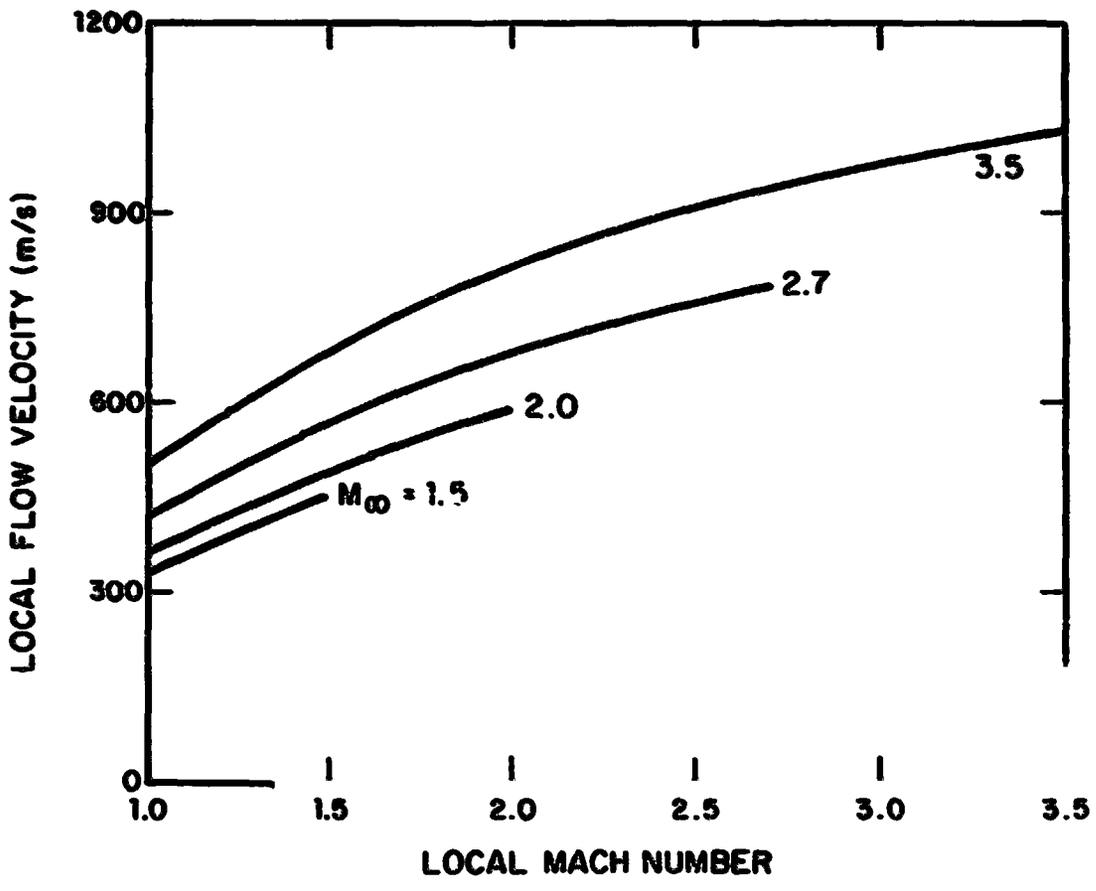

FIG. 23 FLUID VELOCITY OVER HEAT SHIELD DURING REENTRY

In Fig. 24 is shown the *maximum* local density encountered during reentry, displayed as a function of the local Mach number. At $M_{local} = 1.5$, $\rho_{local} = 0.618$ kg/m^3 ($1.2 \cdot 10^{-3}$ slugs/ft^3), so the density parameter μ for the heat shield is

$$\mu = \frac{\rho b}{m}$$

$$= \frac{(1.2 \cdot 10^{-3})(2.5)}{0.012}$$

$$= 0.25$$

From Fig. 7 of Dowell (1966), using M = 1.5 and $\mu = 0.25$, we obtain for the critical flow velocity

$$\frac{U_{cr}}{c_{min}} \doteq 2.5$$

solving for c_{min}, and using $U_{cr} = 640$ m/sec as calculated above, we get

$$c_{min} = 268 \text{ m/sec } (880 \text{ ft/sec})$$

From Fig. 22, the required stiffness is, assuming Eh = 0,

$$D = 1980 \text{ N·m } (1460 \text{ ft·lb})$$

If we assume Eh = 17500 kN/m (10^5 lb/in), we get

$$D = 362 \text{ N·m } (267 \text{ ft·lb})$$

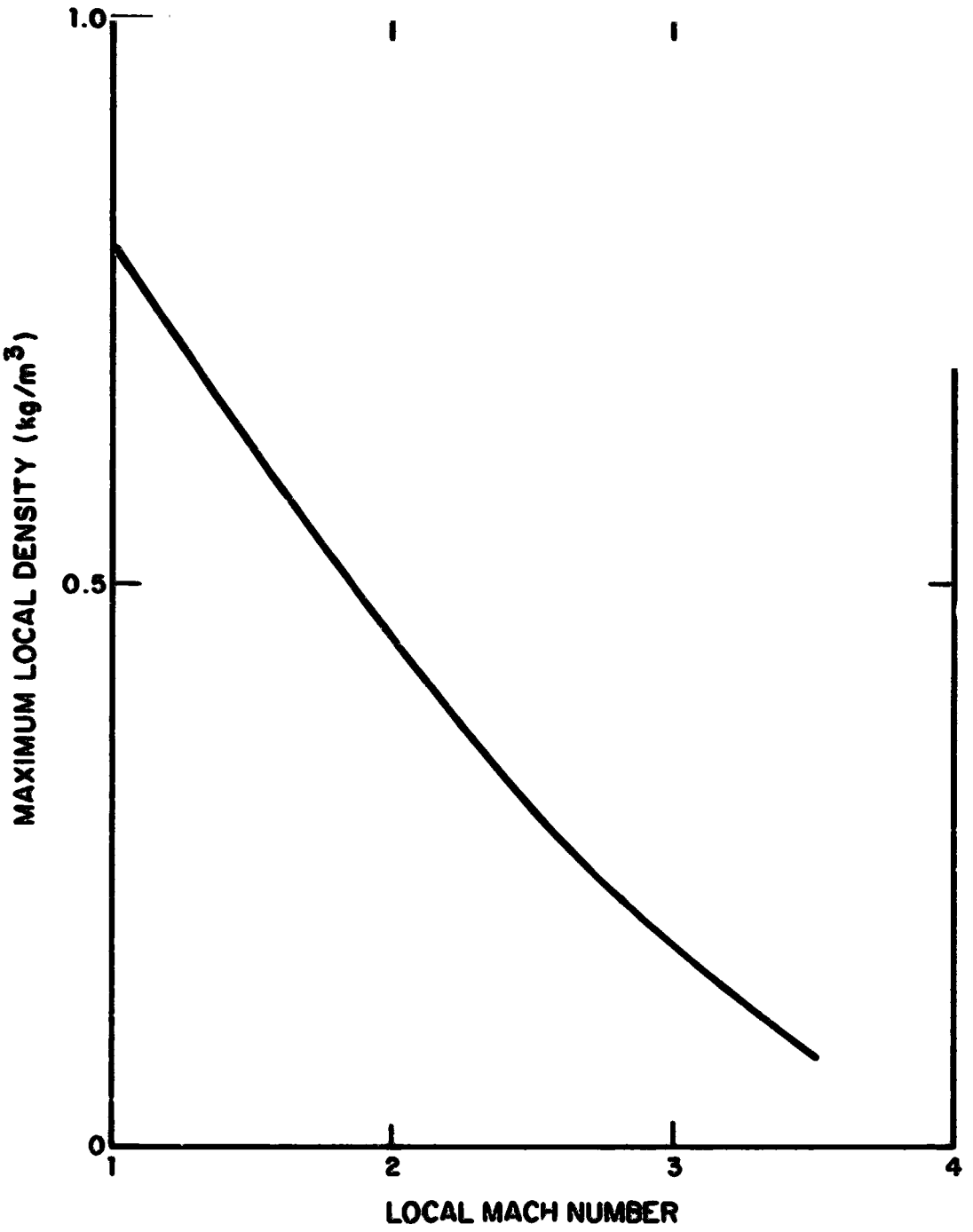

FIG. 24. MAXIMUM LOCAL FLUID DENSITY DURING REENTRY VS LOCAL MACH NUMBER

5.1.2 Stiffness Required to Prevent Flutter at High Supersonic Speeds

For $M \geq 1.5$, the stability boundary is given by Eq. 13. This equation contains $(q/\beta)_{local}$ rather than U_{local}. In Fig. 25 Eq. 13 is plotted as q/β vs. D for $\Delta p = 0$ and 28 kN/m^2 (4 psi). Note that, when $\Delta p > 0$, one can suppress flutter by *decreasing* the bending stiffness D. This is not possible when $\Delta p = 0$, however, and is not possible for any Δp at low supersonic Mach numbers. Making the heat shield more flexible is not, therefore, a feasible flutter "fix."

Figure 26 displays the maximum value of $(q/\beta)_{local}$ encountered during reentry as a function of reentry Mach number. (At all reentry Mach numbers, this maximum occurs at the angle of attack at which $M_{local} = 1.5$.) The peak value of $(q/\beta)_{local}$ is, from the figure,

$$(q/\beta)_{local} = \quad 10^4 \quad kN/m^2 \ (2170 \ lb/ft^2)$$

From Fig. 25, assuming conservatively that $\Delta p = 0$, the required bending stiffness is

$$D = \quad 2260 \ N \cdot m \quad (1670 \ ft \cdot lb)$$

This required stiffness is greater than either of the values calculated for $M_{local} \leq 1.5$, so it is the controlling stiffness requirement for prevention of flutter during reentry.

To express this bending stiffness requirement in more easily comprehensible terms, we have calculated the thickness of a homogeneous aluminum plate having this bending stiffness. Assuming for aluminum $E = 6.9 \cdot 10^7$ kN/m^2 (10^7 psi), the thickness is

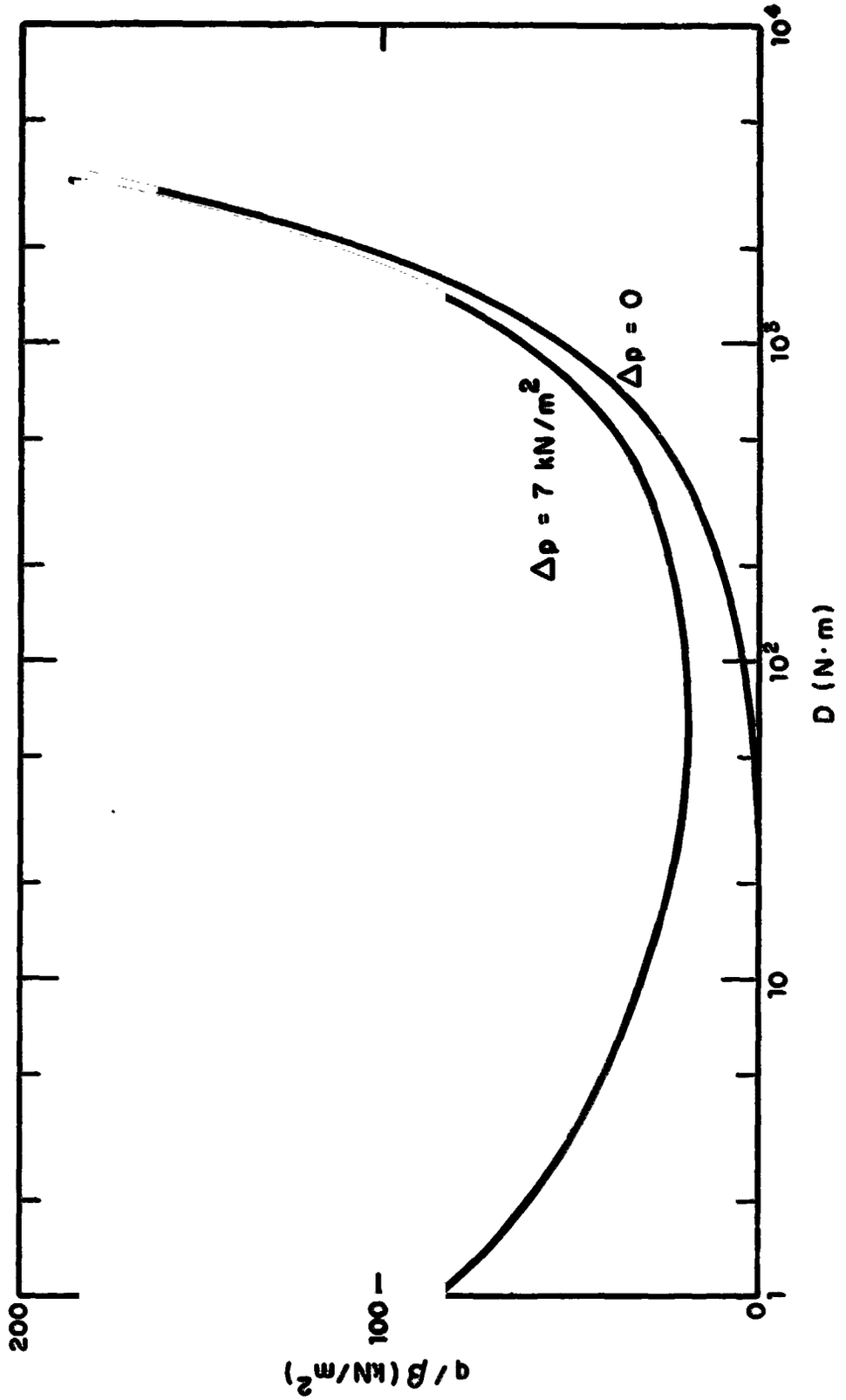

FIG. 25. CRITICAL VALUE OF q/β VS BENDING STIFFNESS

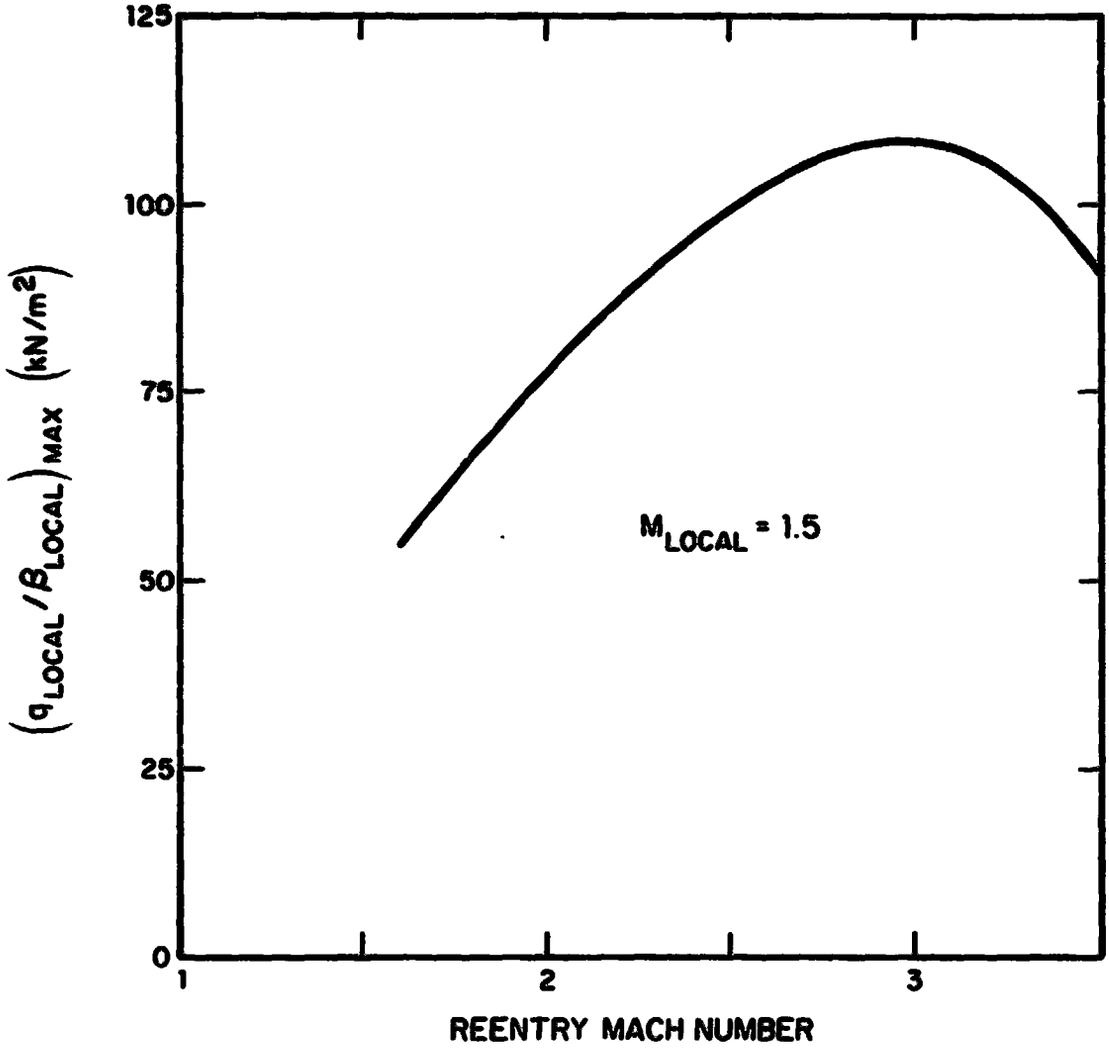

FIG. 26. MAXIMUM LOCAL VALUE OF q/β DURING REENTRY

$$h = \left[\frac{12(1-\nu^2)D}{E}\right]^{1/3}$$

$$= 0.710 \text{ cm } (0.28 \text{ in})$$

This is a substantial thickness. The estimate of stiffness required is expected to be somewhat conservative, because in deriving Eq. 13, aerodynamic damping was neglected (i.e., $\mu = 0$), whereas in fact, $\mu = 0.25$.

Nevertheless, the fabric heat shield cannot be expected to be as stiff as an aluminum plate 0.710 cm thick. As a result, we predict that the heat shield will flutter during reentry.

5.2 Concepts for Flutter Suppression

The 3% scale model studies (both theory and experiment) suggest that a static pressure differential or other means of introducing in-plane tension into the heat shield is beneficial in suppressing flutter. The theory also suggests that increasing the bending stiffness is helpful at both low and high Mach numbers. Because of the requirement that the rocket nozzle be swiveled during ascent, the amount of radial stiffness that can be allowed is limited. We are led, therefore, to consider orthotropic structures with greater circumferential than radial bending stiffness. All the flutter suppression concepts that have been considered to date include one or both of these two ingredients (i.e., in-plane tension and orthotropic bending stiffness) in some form or other. Before discussing specific designs, we will outline briefly the modifications required in the low and high Mach number theories to handle orthotropic bending stiffness (both theories already incorporate Δp).

All that is required at low Mach numbers is to modify Eq. 12 for c_{min} to include orthotropic bending stiffness. The aerodynamic theory remains unchanged. Introducing D_x and D_y as the circumferential and radial bending stiffnesses, the square of the minimum wavespeed becomes

$$c^2_{min} = 2\pi^2 \left(\frac{D_x}{mb^2}\right)^{1/2} \left[D_y + \frac{N_y b^2}{\pi^2}\right]^{1/2} + \frac{N_x}{m} \qquad (14)$$

By suitable choices of D_x, D_y and N_x, N_y (which may be introduced by a pressure differential or by other means), one can make c_{min} sufficiently large to prevent flutter. An application of this formula to a specific design concept is discussed in Appendix B.

The high Mach number theory ($M_{local} > 1.5$) is based on the low aspect ratio (large length/width ratio) flat plate theory presented in Dowell and Ventres (1970). This can easily be extended to include D_x, D_y, N_x and N_y by changing the definitions of certain terms in the equations presented there.

5.3 Proposed Design Modifications

Design concepts considered so far, as well as others recommended as deserving additional study are listed below, along with comments where appropriate.

(1) Present Heat Shield With In-Plane Tension

The requirement that the heat shield detach from the aft skirt at water impact presently limits the maximum acceptable in-place tension to the equivalent of 2 kN/m^2 (0.3 psi). Unless this limitation is removed (as, for exampel, by using pyrotechnics to actively sever the heat shield prior to splash-down), in-place tension, by itself, does not merit further consideration.

(2) Present Heat Shield With In-Plane Tension and Circumferential Stiffness via Circumferential Hoops

Setting $D_y = 0$ in Eq. (14) (zero radial stiffness), we obtain

$$c^2_{min} = 2\pi \left(\frac{D_x N_y}{m^2 b^2} \right)^{1/2} + \frac{N_x}{m} \qquad (15)$$

This equation has been incorporated into a design procedure (see Appendix B) for selecting the required stiffness D_x and in-plane tensions N_x, N_y (expressed as an equivalent Δp). The required tension is apparently larger than desirable from a structural standpoint, but on the other hand, the theory used to establish the required tension may be quite conservative. This concept deserves further consideration.

(3) Present Heat Shield With Orthotropic Bending Stiffness in Both Radial and Circumferential Directions via Circumferential Hoops and Radial Stays

The governing equation for the wavespeed is Eq. (14). No detailed calculations have been made as yet, but it is apparent that some tension must be retained in the fabric to prevent flutter of the fabric between the stiffening members.

(4) Nonconventional Structures, Such as an "Inner Tube" Placed Beneath the Fabric Heat Shield

The pressure required to stabilize the heat shield will be quite high, especially if the heat shield is bulged outward during reentry. Thus, the "inner tube" may have to be inflated (or the pressure increased) after the SRB separates from the Shuttle Orbiter. The mechanical arrangement must be such that tension is induced in the heat shield itself (not merely in the inner

tube) to prevent "local flutter" of the heat shield (i.e., flapping against the wall of the inner tube).

This concept requires further study. Bulging the heat shield outward introduces an additional unknown aspect to the problem, because the local flow field will no longer closely resemble that encountered in the wind tunnel tests completed so far.

6. RECOMMENDED PROGRAM OF EXPERIMENTS

In this section, we outline a program of vibration tests and wind tunnel tests that are required to determine how the heat shield can be modified to avoid flutter during reentry. These experiments are needed because the theory, by itself, does not afford an acceptable level of confidence in determining whether or not a specific heat shield design will flutter. The theory does, however, provide valuable insight into the mechanism of the instability, and helps to identify promising flutter suppression concepts.

A detailed proposal for wind tunnel aeroelastic tests at 6% scale has already been submitted to NASA MSFC.* In this section, therefore, only salient features of the proposed program will be discussed.

6.1 Aeroelastic Scaling Parameters

A formal analysis of the heat shield for the purpose of identifying scaling parameters for aeroelastic and acoustic tests has been carried out, and is reported in Volume II of this report. The appropriate scaling parameters also appear, of course, in the flutter theory presented in Section 4. The scaling parameters are listed below (L denotes a typical length).

$$M, \frac{EhL^2}{D}, \frac{N_x L^2}{D}, \frac{N_y L^2}{D}, \frac{qL^3}{D}, \frac{\rho L}{m}$$

The significance of each as regards the design and construction of an aeroelastically scaled model and the conduct of the wind tunnel tests will be discussed in turn.

---

*BBN Proposal Number P77-NCT-70, Nov. 1976, revised Feb. 1977, as P77-NCT-70a.

M is the Mach number of the flow over the face of the heat shield. According to the wedge flow analogy discussed in Section 2, the local Mach number is the same at all points on the heat shield, and is related to the free stream (reentry or wind tunnel test section) Mach number as shown in Fig. 8. However, this model of the flow adjacent to the heat shield is supported by a limited amount of data, and is in any event a simplification of the situation that actually exists. To model the flow field accurately, the wind tunnel tests should be conducted by mounting the aeroelastically scaled heat shield models on a geometrically scaled model of the entire aft end of the SRB.

EhL^2/D is a ratio of two structural parameters of the heat shield, the in-plane stiffness Eh and the bending stiffness D. This parameter is not very important in determining the stability of the present heat shield design (see Section 5.1.1), but might become significant if the design were modified substantially. In any event, EhL^2/D can be matched between model and full scale by proper selection of the material of which the model is constructed.

N_xL^2/D and N_yL^2/D are the in-plane tension loading parameters. In-plane tension can be introduced by imposing a pressure differential Δp across the heat shield, or by mechanical means. If the tension is solely due to Δp then $N_x = \Delta pR/2$, and $N_y = \Delta pR$, where R is the sag radius. In this situation, the two parameters reduce to one. Because $R \sim L$, we may write this one parameter as $\Delta pL^3/D$. In a wind tunnel test, Δp can be set at any desired value by controlling the pressure within the cavity behind the heat shield. If N_x and/or N_y are introduced by mechanical means at full scale, similar methods may be used in the model. Thus, these parameters impose no conceptual difficulty in scaling.

The remaining two scaling parameters, qL^3/D and $\rho L/m$, determine the bending stiffness and surface mass density required of the model heat shield. Because most wind tunnels operate at a

fixed total temperature, the test section flow density and dynamic pressure cannot be separately controlled. Therefore, while both of these parameters can be scaled at *any single test section Mach number* by appropriate choices for D and m, different values of D and m will be required at other Mach numbers. In consequence, perfect aeroelastic scaling is not possible at all Mach numbers. The heat shield models can be constructed, however, so as to make the scaling conservative (i.e. so as to *decrease* the dynamic pressure at which the model flutters). Theory indicates that the dynamic pressure at which flutter occurs generally increases as the parameter $\rho L/m$ increases. Conservative scaling would be achieved, therefore, if $(\rho L/m)_{model} \leq (\rho L/m)_{full\ scale}$ at all test section Mach numbers.

6.2 Vibration Tests

A series of vibration tests on both the scale model heat shields and on the full scale heat shield are recommended prior to wind tunnel entry. Such tests are recommended in NASA Space Vehicle Design Criteria Document on Panel Flutter, NASA SP-8004. The purpose of these tests is to verify that the wind tunnel model is dynamically similar to the full scale article, and to verify that the theoretical flutter model adequately represents the *in-vacuo* vibration behavior of both the model and the full scale structure.

These tests will be carried out by shaking the heat shield locally at various frequencies, and measuring the amplitude and speed of the waves that propagate around the annulus. If a complete full scale heat shield (24 segments) is not available, meaningful results could probably be achieved with only 4 or 5 segments.

6.3 Wind Tunnel Tests

The wind tunnel tests should be conducted at test section Mach numbers between 2 and 3.5, because this is the most critical range with regard to flutter. A range of dynamic pressures should be employed, with the scaled maximum dynamic pressure reaching or exceeding a level 50% greater than the maximum levels anticipated during reentry (Fig. 2). The angle of attack range should also encompass the range expected during reentry (Fig. 3), but the highest priority should be assigned to those angles at each test section Mach number at which the local Mach number over the heat shield is between 1 and 2.

Testing a rigid heat shield, instrumented for the measurement of local velocities and pressures, over the entire range of Mach numbers and angles of attack would clarify the details of the flow field, and would facilitate comparisons between theory and experiment for the aeroelastic tests to follow.

It would be desirable, but not absolutely essential, to provide means for varying the angle of attack between 90° and 180° without shutting down the tunnel. This would allow the tunnel to be started at a reduced dynamic pressure with the angle of attack set at 180° (heat shield facing the flow), where flutter is not anticipated. Two test procedures are then possible. The model can be rotated to the desired angle of attack, and then the dynamic pressure increased until flutter is encountered, or until q_{max} is reached. This procedure would assure that the flutter boundary is encountered only once. Alternatively, the dynamic pressure can first be raised to the desired value, and then the model can be rotated through the desired angle of attack range. Depending upon the heat shield design, two flutter boundaries may be encountered, one where flutter commences,

another where flutter ceases. This is because the local Mach number passes through the most critical range ($1 < M_{local} < 2$) at intermediate values of α (see Figs. 8, 20, and 21).

Measuring the motion of the model heat shields presents some difficulty, because the amplitude of the expected oscillations are on the order of the width of the annulus, and the heat shields will be very light in weight. An optical sensing system that adds no mass whatsoever to the heat shield is described in the proposal. High speed films will be useful in studying the details of the oscillations, as they were in the AEDC tests. Other instrumentation for measuring flow velocity and dynamic pressure will be conventional.

Several flutter suppression concepts should be tested, although not all need be tested over the entire range of M, q, and α. Furtheremore, three versions of each "fix" should be constructed and tested. These will have graduated levels of structural stiffness (or some other key parameter, such as internal pressure in the case of the inflated "inner tube" concept). This procedure will mak it possible to interpolate or extrapolate the data to determine the stiffness level required to suppress flutter during reentry. The three levels of stiffness need not correspond to values that would be acceptable in full scale; it would be more informative to discover the actual stiffness required to prevent flutter, even though this level be unacceptable on other grounds, than to complete the test program without having tested a flutter-free heat shield.

7. SUMMARY AND CONCLUSIONS

The oscillations observed in the AEDC wind tunnel tests on a 3% scale model of the SRB have been traced to aeroelastic instability of the heat shield. A flutter theory based on a simplified geometrical model of the annular heat shield shows relatively good agreement with experiment as to the frequency, wavelength and wavespeed of the oscillations, and the range of angles of attack at which the oscillations are most severe.

It was not possible to apply the same theory directly to the full scale SRB heat shield to determine whether or not it would flutter during reentry, because the requisite mechanical properties of the heat shield are not known. Instead, the bending stiffness required to prevent flutter was calculated. This stiffness was found to be far greater than the fabric heat shield could possibly possess in its present form. On this basis, the SRB heat shield is expected to flutter during reentry.

Theory indicates that flutter can be suppressed by providing sufficient in-plane tension in the heat shield, or by increasing its bending stiffness (the present heat shield is a limp fabric structure). In-plane tension can be supplied by placing a static pressure differential between the inner and outer surfaces of the heat shield, or by any equivalent means. The amount of tension, acting alone, that would be required to stabilize the heat shield would be quite large. Combined tension and bending stiffness is suggested as a better means of suppressing flutter.

A program of experiments, including vibration tests on both the full scale heat shield (or a portion thereof), and on aeroelastically scaled models of the heat shield, and a series of aeroelastic wind tunnel tests is proposed in order to determine a design modification or "fix" that will stabilize the heat shield.

The wind tunnel tests should be conducted at test section Mach numbers between 2 and 3.5. Dynamic pressure should be increased until flutter is encountered, or until maximum tunnel dynamic pressure is reached. Maximum tunnel dynamic pressure should correspond at model scale to a level 50% greater than the maximum pressure expected during reentry. The tests should be carried out on a geometrically scaled model of the aft end of the SRB. This model should be rotated through the full range of angles of attack expected during reentry, although highest priority should be assigned those angles of attack that produce local Mach numbers, over the face of the heat shield, between 1 and 2. This Mach number range is most critical with regard to flutter. Each flutter suppression concept should be tested in three different versions, having different levels of stiffness. This procedure will make it possible to interpolate or extrapolate the data to determine the minimum stiffness required to prevent flutter during reentry.

APPENDIX A

ELASTIC CONSTANTS OF THE 3% SCALE MODEL HEAT SHIELDS USED IN THE WIND TUNNEL TESTS AT AEDC

Using data provided by R.W. Walker of NASA MSFC (private communication), the in-plane stiffness Eh, and compressional wave speed $\sqrt{Eh/m}$ were calculated for the model heat shields used in the wind tunnel tests at AEDC. Walker performed uniaxial pull tests on rectangular samples of material cut from the heat shields at two orientations, one radial, and the other circumferential. He supplied graphic recordings of force vs elongation. These curves were not linear, so judgement had to be exercised in deciding at what strain level (or elongation) to measure the slope. In consequence, the valves calculated for Eh and $\sqrt{Eh/m}$ are at best crude estimates of the equivalent linear elastic constants of the heat shields.

1. Materials Used at $M_\infty = 2.75$

A. Lightweight Nylon Impregnated with Rubber:

	Sample Orientation	
	Radial	Circumferential
h	.015 cm	
m	0.20 kg/m^2	
Eh	$1.8 \cdot 10^4$ N/m	$2.3 \cdot 10^4$ N/m
Eh/m	300 m/s	335 m/s

B. Polyester Cloth

	Sample Orientation	
	Radial	Circumferential
h	.025 cm	
m	.097 kg/m^2	
Eh	$1.1 \cdot 10^6$ N/m	$3.7 \cdot 10^3$ N/m
Eh/m	335 m/s	195 m/s

2. Materials Used at $M_\infty = 3.50$

A. Heavy Nylon Impregnated with Rubber:

	Sample Orientation	
	Radial	Circumferential
h	.025 cm	
m	.028 kg/m^2	
Eh	$1.5 \cdot 10^6$ N/m	$1.5 \cdot 10^6$ N/m
Eh/m	231 m/s	231 m/s

B. Polyester Cloth

	Sample Orientation	
	Radial	Circumferential
h	.025 cm	
m	.097 kg/m^2	
Eh	$9.3 \cdot 10^3$ N/m	$3.5 \cdot 10^3$ N/m
Eh/m	309 m/s	190 m/s

APPENDIX B

HEAT SHIELD STIFFENED BY CIRCUMFERENTIAL HOOPS AND IN-PLANE TENSION

As presently conceived, the heat shield is a limp fabric curtain. The curtain covers an annular opening having an outer diameter of 208 inches, and an inner diameter of 148 inches. Enough slack is provided for so that the fabric can assume a sag radius of about 15 inches.

One way to improve the aeroelastic stability of the heat shield is to stiffen it by

(1) sewing circumferential rings or hoops into the fabric at equally spaced radial increments, and
(2) applying an in-plane tension to the fabric.

At low supersonic Mach numbers ($1 < M < 1.5$), the criteria for stability is that the minimum *in-vacuo* wavespeed exceed 268 m/s (880 ft/sec). (See Section 5.1.1.) The minimum wavespeed in the reinforced heat shield is given by Eq. (15),

$$c^2_{min} = 2\pi \left(\frac{D_x N_y}{m^2 b^2}\right)^{1/2} + \frac{N_x}{m} \qquad \text{(B-1)}$$

and the wavelength at which this minimum wavespeed occurs is

$$\left(\frac{\ell}{2b}\right)_{min} = \left(\frac{D_x \pi^2}{N_y b^2}\right)^{1/4} . \qquad \text{(B-2)}$$

If the inplane tensions N_x and N_y are caused by static pressure differential, then $N_x = N_y/2$ (see Eq. [3]). Therefore,

$$c^2_{min} = 2\pi \left(\frac{D_x N_y}{m^2 b^2}\right)^{1/2} + \frac{N_y}{2m}$$

It is convenient to re-arrange this expression as follows:

$$c_{min}^2 = 2\pi \left(\frac{N_y}{m}\right) \left(\frac{D_x}{N_y b^2}\right)^{1/2} + 1/2 \left(\frac{N_y}{m}\right) \qquad \text{(B-3)}$$

If the critical wavelength greatly exceeds the width of the heat shield, then the "straightened out" geometrical model upon which these calculations are based (Section 4.2) becomes inconsistent Hence restrict $\ell/2b$ to be less than, say, 2.11. From Eq. (B-2), this is equivalent to requiring that

$$\frac{D_x}{N_y b^2} \leq \frac{1}{\pi^2} \left(\frac{\ell}{2b}\right)^4$$

$$= 2 \quad .$$

Inspection of Eq. (B-3) shows that large values of $D_x/N_y b$ are advantageous, in that they reduce the in-plane tension needed to meet the required c_{min}. Thus set

$$\frac{D_x}{N_y b^2} = 2. \qquad \text{(B-4)}$$

Eq. (B-3) becomes

$$c_{min}^2 = (2\pi\sqrt{2} + 1/2) \left(\frac{N_y}{m}\right)$$

Solving for the required $\frac{N_y}{m}$,

$$\frac{N_y}{m} = \frac{c^2_{min}}{2\pi\sqrt{2} + 1/2} \qquad \text{(B-5)}$$

From Eq. (B-4), the associated circumferential bending stiffness is

$$D_x = 2\left(\frac{N_y}{m}\right) mb^2$$

or,

$$\frac{D_x}{mb^2} = \frac{2\, c^2_{min}}{2\pi\sqrt{2} + 1/2} \qquad \text{(B-6)}$$

The circumferential bending stiffness D_x is due entirely to the hoops. If N hoops are employed, each having the same beam bending stiffness EI, then

$$D_x = \frac{NEI}{b}$$

On the other hand, the mass/unit area m depends on both the surface mass density of the fabric and the mass of the hoops:

$$m = m_{fabric} + \frac{M_{hoops}}{A_s}$$

where A_s is the surface area of the heat shield, taking the sag radius into account.

If we use tubular hoops with wall thickness t, then

$$I = \pi r^3 t$$

So

$$D_x = \frac{NE\pi r^3 t}{b}$$

Solving for r,

$$r = \left(\frac{D_x b}{NE\pi t}\right)^{1/3}$$

Let L be the average circumference of the hoops and ρ_h be the mass density of the material of which they are constructed. Then their total mass is

$$M_{hoops} = 2\pi rtL\rho_h$$

$$= 2N\pi \left(\frac{D_x b}{NE\pi t}\right)^{1/3} tL\rho_h$$

So the mass/unit area of the reinforced heat shield is

$$m = m_{fabric} + 2N\pi\left(\frac{D_x b}{NE\pi t}\right)^{1/3} tL\rho_h / A_s \qquad \text{(B-7)}$$

Eqs. (B-6) and (B-7) can be solved iteratively for the mass/unit area m and the required bending stiffness D_x. The procedure is to assume a value for m ($m = m_{fabric}$ is a good starting assumption), compute D_x from Eq. (B-6), then compute a new value for m from Eq. (B-7), and so on.

For example, if we use four aluminum tubes with a wall thickness of 0.127 cm (0.05 in), and assume that $m_{fabric} = 1.88$ kg/m^2 (.012 slugs/ft^2), then

$$N = 4$$

$E = 7.10^7$ kN/m^2. (10^7 psi)

$\rho_h = 277$ kg/m^3 (.00311 slugs/in^3)

and we obtain

$m = 4.04$ kg/m^2 (0.0257 slugs/ft^2)

$D_x = 3.59 \cdot 10^4$ N·m ($2.65 \cdot 10^4$ ft·lb)

The radius and wall thickness of the 4 tubular aluminum hoops are:

$r = 2.9$ cm (1 15 in)

$t = 0.13$ cm (0.05 in)

The required in-plane tension N_y is, from Eq. (B-5),

$N_y = 20.0$ kN/m (2120 lb/ft)

The pressure differential required to establish this tension is

$$\Delta p = \frac{N_y}{R}$$

$$= 81.4 \text{ kN/m}^2 \quad (11.8 \text{ psi})$$

LIST OF SYMBOLS

A_s = surface area of heat shield

b = Width of annular heat shield (Fig. 11).

c = Wavespeed.

c_{min} = Minimum wavespeed.

c_o = Minimum *in-vacuo* wavespeed in a flat plate.

D = Bending stiffness.

E = Young's modulus.

Eh = In-plane stiffness.

f = Frequency.

F(η) = Aerodynamic integral in Eq. (9) (from Dowell [1964]).

h = Thickness of model heat shield.

i = $\sqrt{-1}$

ℓ = Wavelength.

M = Mach number.

M_{local} = Mach number over face of heat shield.

M_∞ = Test section or reentry Mach number.

m = mass/unit area of heat shield.

N_x = Stream-wise in-plane tension.

N_y = Cross-stream in-plane tension.

P = Pressure.

q = Dynamic pressure ($\frac{1}{2}\rho U^2$)

R = Sag radius of heat shield (Fig. 11)

t = Time.

V = Flow velocity.

w = Transverse deflection of heat shield.

x = Stream-wise coordinate (Fig. 11).

y = Cross-stream coordinate (Fig. 11).

α = Wavenumber ($2\pi/\ell$)

β = $\sqrt{M^2-1}$

Γ = Dimensionless constant defined in Eq. (10).

Δp = Static pressure differential.

η = Dimensionless variable defined in Eq. (8).

μ = Normalized flow density ($\rho b/m$).

ν = Poisson's ratio.

ρ = Flow density.

ψ = Airy stress function in Eq. (2).

Superscripts

$*$ = Flow velocity or wavespeed d vided by c_o (minimum *in-vacuo* wavespeed in a flat plate).

Subscripts

cr = Critical value or value at which flutter occurs.

min = Minimum value.

∞ = Free-stream value.

REFERENCES

Dixson, S.C. (1966), "Comparison of Panel Flutter Results from Approximate Aerodynamic Theory with Results from Exact Inviscid Theory and Experiment," NASA TN D-3649, May 1966.

Dowell, E.H. (1964), "The Flutter of Very Low Aspect Ratio Panels," AFOSR 64-1723, July 1964.

Dowell, E.H. (1966), "Flutter of Infinitely Long Plates and Shells. Part I: Plate," *AIAA Journal* 4 (8), pp. 1370-1377, Aug. 1966.

Dowell, E.H. (1969), "Nonlinear Flutter of Curved Plates," *AIAA Journal* 7 (3), pp. 424-431, March 1969.

Dowell, E.H. (1970), "Nonlinear Flutter of Curved Plates II", *AIAA Journal* 5 (10), pp. 261-263, Feb. 1970.

Dowell, E.H. (1972), "Panel Flutter," NASA SP-8004, July, 1964 (revised June, 1972).

Dowell, E.H. (1975), *Aeroelasticity of Plates and Shells*, Noordhoff International Publishing Co., Leyden, 1975.

Dowell, E.H., and Ventres, C.S. (1970), "Flutter of Low Aspect Ratio Plates," *AIAA Journal* 8 (6), pp. 1162-1164, June, 1970.

Dym, C.L. (1974), *Introduction to the Theory of Shells*, Pengamon Press, Oxford, 1974, p. 71.

Gallaboff, Z. (1976), "Reentry Trajectory Data for Generation of SRB Acoustic Environments," Memo, NASA MSFC, Aug. 1976.

Liepman, H.W., and Roshko, A., (1957). *Elements of Gasdynamics*, John Wiley and Sons, Inc., New York, 1957.

NACA (1953), "Equations, Tables, and Charts for Compressible Flow," NACA Report 1135, 1953.

Porter, J.H., Jr., (1976), "An Aero-Acoustic Test of a 3-Percent Scale SRB with Various Flexible Heat Shields and Aero-Fixes," AEDC-DR-76-11 Von Karman Gas Dy-amics Facility Arnold Engineering Development Center, Feb. 1976.

Ventres, C.S., and Kang, C.K. (1973), "Large Amplitude Flutter of a Low Aspect Ratio Panel at Low Supersonic Speeds: Comparison of Theory and Experiment," Princeton University AMS Report No. 1116, prepared under Contract NAS 8-28577 for NASA MSFC, August 1973.